

Global constraints on non-standard neutrino interactions with quarks and electrons

Pilar Coloma,^a M.C. Gonzalez-Garcia,^{b,c,d} Michele Maltoni,^a João Paulo Pinheiro^c and Salvador Urrea^e

^a*Instituto de Física Teórica (IFT-CFTMAT), CSIC-UAM, Calle de Nicolás Cabrera 13–15, Campus de Cantoblanco, E-28049 Madrid, Spain*

^b*C.N. Yang Institute for Theoretical Physics, Stony Brook University, Stony Brook, NY 11794-3840, U.S.A.*

^c*Departament de Física Quàntica i Astrofísica and Institut de Ciències del Cosmos, Universitat de Barcelona, Diagonal 647, E-08028 Barcelona, Spain*

^d*Institució Catalana de Recerca i Estudis Avançats (ICREA), Pg. Lluís Companys 23, E-08010 Barcelona, Spain*

^e*Instituto de Física Corpuscular (IFIC), CSIC-UV, Edificio Institutos de Investigación, Calle Catedrático José Beltrán 2, E-46980 Paterna, Spain*

E-mail: pilar.coloma@ift.csic.es,
maria.gonzalez-garcia@stonybrook.edu, michele.maltoni@csic.es,
joaopaulo.pinheiro@fqa.ub.edu, salvador.urrea@ific.uv.es

ABSTRACT: We derive new constraints on effective four-fermion neutrino non-standard interactions with both quarks and electrons. This is done through the global analysis of neutrino oscillation data and measurements of coherent elastic neutrino-nucleus scattering (CE ν NS) obtained with different nuclei. In doing so, we include not only the effects of new physics on neutrino propagation but also on the detection cross section in neutrino experiments which are sensitive to the new physics. We consider both vector and axial-vector neutral-current neutrino interactions and, for each case, we include simultaneously all allowed effective operators in flavour space. To this end, we use the most general parametrization for their Wilson coefficients under the assumption that their neutrino flavour structure is independent of the charged fermion participating in the interaction. The status of the LMA-D solution is assessed for the first time in the case of new interactions taking place simultaneously with up quarks, down quarks, and electrons. One of the main results of our work are the presently allowed regions for the effective combinations of non-standard neutrino couplings, relevant for long-baseline and atmospheric neutrino oscillation experiments.

KEYWORDS: Neutrino Mixing, Non-Standard Neutrino Properties, Neutrino Interactions

ARXIV EPRINT: [2305.07698](https://arxiv.org/abs/2305.07698)

Contents

1	Introduction	1
2	Formalism	5
2.1	Neutrino oscillations in the presence of NSI	6
2.1.1	Matter potential in atmospheric and long-baseline neutrinos	9
2.1.2	Matter potential for solar and KamLAND neutrinos	10
2.1.3	Departures from adiabaticity in presence of NSI	12
2.2	Neutrino detection cross sections in the presence of NSI	14
2.2.1	Neutrino-electron elastic scattering	14
2.2.2	SNO neutral-current cross-section	16
2.2.3	Coherent elastic neutrino-nucleus scattering	16
3	Results	17
3.1	Simulation details	17
3.2	New constraints on NSI with electrons	20
3.3	Updated constraints on NSI with quarks	22
3.4	Constraints on NSI with quarks and electrons: effective NSI in the Earth	27
3.5	Present status of the LMA-D solution	31
4	Summary	33

1 Introduction

The minimal global description of the bulk of data gathered in experiments detecting the interactions of solar and atmospheric neutrinos, and of neutrinos produced in nuclear reactors and in particle accelerators, requires three neutrino states with distinct masses which are non-trivial admixtures of the three flavour neutrino states of the Standard Model (SM). This implies that lepton flavour oscillates with a wavelength which depends on distance and energy [1, 2] as required to explain the data, see ref. [3] for an overview. This is one of the most direct indications of physics beyond the Standard Model (BSM).

Given the excellent ability of the SM in explaining the interactions of fundamental particles through the electromagnetic, weak, and strong interactions, it is reasonable to assume that the SM is an effective theory and that new physics (NP) effects are suppressed at low energies. Generic BSM physics can then be introduced in a model-independent manner through a tower of effective operators, suppressed by the heavy NP scale. Interestingly enough, neutrino masses arise in this framework from the unique dimension-five operator consistent with the SM gauge symmetry and particle contents, and therefore can be argued to be the first signal of BSM physics. At next order in the operator expansion we find

dimension-six four-fermion operators. Those involving neutrino fields would affect the production, propagation, and detection of neutrinos — the so-called Non-Standard neutrino Interactions (NSI). In this work we focus on operators leading to purely vector or axial-vector interactions (for recent works including additional operators with different Lorentz structures see for example refs. [4–7]). Generically these can be classified in charged-current (CC) NSI

$$\mathcal{L}_{\text{NSI,CC}} = -2\sqrt{2}G_F \sum_{f,f',\alpha,\beta} \varepsilon_{\alpha\beta}^{ff',P} (\bar{\ell}_\alpha \gamma_\mu P_L \nu_\beta) (\bar{f} \gamma^\mu P f') + \text{h.c.} \quad (1.1)$$

and neutral-current (NC) NSI

$$\mathcal{L}_{\text{NSI,NC}} = -2\sqrt{2}G_F \sum_{f,P,\alpha,\beta} \varepsilon_{\alpha\beta}^{f,P} (\bar{\nu}_\alpha \gamma^\mu P_L \nu_\beta) (\bar{f} \gamma_\mu P f). \quad (1.2)$$

In eqs. (1.1) and (1.2), f and f' refer to SM charged fermions, ℓ denotes a SM charged lepton and P can be either a left-handed or a right-handed projection operator (P_L or P_R , respectively). Moreover the normalization of the couplings is deliberately chosen to match that of the weak currents in the SM, so the values of $\varepsilon_{\alpha\beta}^{f,P}$ indicate the strength of the new interaction with respect to the Fermi constant, G_F . The corresponding vector and axial-vector combinations of NSI coefficients are defined as:

$$\varepsilon_{\alpha\beta}^{f,V} \equiv \varepsilon_{\alpha\beta}^{f,L} + \varepsilon_{\alpha\beta}^{f,R} \quad \text{and} \quad \varepsilon_{\alpha\beta}^{f,A} \equiv \varepsilon_{\alpha\beta}^{f,L} - \varepsilon_{\alpha\beta}^{f,R}. \quad (1.3)$$

Precise measurements of meson and muon decays place severe constraints on the possible strength of CC NSI (see for example refs. [4, 8–10]). Conversely, NC NSI are much more difficult to probe directly, given the intrinsic difficulties associated to neutrino detection via neutral currents. A priori, the requirement of gauge invariance would generate similar operators in the charged lepton sector, in severe conflict with experimental observables [11, 12]. However, such bounds may be alleviated (or evaded) in NP models in which NC NSI are generated by exchange of neutral mediators with masses well below the EW scale (for a recent review on viable NSI models see, e.g., ref. [13]). It is in these scenarios that one can envision observable effects in present and future neutrino experiments. Several models have been proposed, involving new gauge symmetries and light degrees of freedom, that would give rise to relatively large NC NSI. These include, for example, models where the NSI are generated from the Z' boson associated to a new $U(1)'$ symmetry [14–21], radiative neutrino mass models involving new scalars [22], or models with leptoquarks [22–24]. Many of these extensions involve a gauge symmetry based on a combination of baryon and lepton quantum numbers, and would therefore induce equal NSI for up and down quarks. However, exceptions to this rule arise, for example, in models with leptoquarks where NSI may be only generated for down-quarks [22, 23]. Similarly it should be stressed that, while many of these models typically lead to diagonal NSI in lepton flavor space, this is not always the case and, depending on the particular extension, sizable off-diagonal NSI may also be obtained (see, e.g., refs. [16, 17, 20]). In order to derive constraints to such a wide landscape of models, the use of the effective operator approach advocated above is extremely useful. For bounds from oscillation data on $U(1)'$ models with diagonal couplings in flavor space, see ref. [25].

In fact, some of the best model-independent bounds on NC NSI are obtained from global fits to oscillation data. These are affected by vector couplings involving fermions present in matter, $\varepsilon_{\alpha\beta}^{f,V}$ with $f \in \{u, d, e\}$, since they modify the effective matter potential [26, 27] felt by neutrinos as they propagate in a medium. In ref. [28] such global analysis was performed in the context of vector NC NSI with either up or down quarks. In ref. [29] the study was extended to account for the possibility vector NC NSI with up and down quarks simultaneously, under the restriction that the neutrino flavour structure of the NSI interactions is independent of the quark type. However, NSI with electrons were not considered.

One important effect of the presence of NSI [26, 30, 31] affecting the neutrino propagation in oscillation experiments is the appearance of a degeneracy leading to a qualitative change of the lepton mixing pattern. This was first observed in the context of solar neutrinos, for which the established standard Mikheev-Smirnov-Wolfenstein (MSW) solution [26, 27] requires a mixing angle θ_{12} in the first octant, while with suitable NSI the data could be described by a mixing angle θ_{12} in the second octant, the so-called LMA-Dark (LMA-D) [32] solution. The origin of the LMA-D solution is a degeneracy in the oscillation probabilities due to a symmetry of the Hamiltonian describing neutrino evolution in the presence of NSI [28, 33–35]. Such degeneracy makes it impossible to determine the neutrino mass ordering by oscillation experiments alone [35] and therefore jeopardizes one of the main goals of the upcoming neutrino oscillation program. Although the degeneracy is not exact when including oscillation data from neutrino propagating in different environments, quantitatively the breaking is small and global fits show that the LMA-D solution is still pretty much allowed by oscillation data alone [28, 29]. A second important limitation of oscillation data is that it is only sensitive to differences in the potential felt by different neutrino flavours. Thus, oscillation data may be used to derive constraints on the differences between diagonal NC NSI parameters, but not on the individual parameters themselves.

Neutrino scattering data is also sensitive to NC NSI as they would affect the interaction rates directly [8, 36–40]. Therefore the combination of oscillation and scattering data may be used to break the LMA-D degeneracy (see for example refs. [32, 41] for early works on this topic). However, such a combination is most effective whenever the scattering cross section also falls in the contact-interaction regime, since otherwise bounds obtained from scattering may be evaded for sufficiently light mediators [15]. As a consequence, for NSI with quarks the most powerful constraints come from measurements of Coherent Elastic Neutrino-Nucleus Scattering [42] ($\text{CE}\nu\text{NS}$), since the momentum transfer is small and therefore apply to a wider class of models, as discussed in refs. [35, 43, 44]. Reference [45] showed the impact obtained from the joint analysis of $\text{CE}\nu\text{NS}$ and oscillation data, considering NSI with only one quark type at a time and using the first measurement of $\text{CE}\nu\text{NS}$ at COHERENT [46]. Our later works [29, 47] subsequently improved over this first analysis by including the latest oscillation data, refining the treatment of COHERENT data [48] and, most importantly, by allowing for NC NSI with up and down quarks simultaneously in the fit, which made the results more general. Moreover, besides lifting the degeneracy, the addition of oscillation and scattering data also allows to obtain separate constraints on the diagonal NSI parameters [45].

The field of $CE\nu NS$ is moving fast. Since the first measurements on CsI, the COHERENT collaboration has reported a separate measurement using an Ar detector [49] and the Dresden-II experiment recently reported a signal using a Ge detector [50]. The combination of $CE\nu NS$ measurements for different target nuclei is highly relevant to lift the LMA-D degeneracy for NC NSI with arbitrary couplings to up and down quarks [36, 38, 43, 51]. Additionally, the combination of data obtained using neutrinos from spallation sources and from reactors may be used to lift degeneracies in NSI flavour space [52]. Therefore, a significant improvement on the bounds for NC NSI with quarks may be expected from the addition of the new datasets that have become recently available.

As mentioned above, the global analyses in refs. [28, 29, 45, 47] only included NSI with quarks. However, there is no reason to avoid the new current to couple to electrons as well. The presence of NSI with electrons would affect not only neutrino propagation but also the interaction cross-section for electron scattering (ES). This would impact the data at both SK and Borexino, and makes the problem much more demanding from the computational point of view. Constraints on NC NSI with electrons were obtained from the analysis of Borexino Phase-II spectrum by the Borexino Collaboration [53] assuming only one NC NSI coupling at a time. Recently, in ref. [54] we performed an analysis of the Borexino Phase-II spectral data including all NC NSI operators involving electrons simultaneously in the fit. Our results showed that the simultaneous presence of several operators significantly deteriorates the resulting bounds. However, the sensitivity of Borexino to NC NSI with electrons stems mainly from their impact on the detection cross section and not from oscillations. Therefore a significant improvement on the final constraints would be expected from the combination with oscillation data from other experiments. While partial analyses for electron NSI using a subset of data have been performed before [32, 40, 41], an analysis using all available neutrino oscillation data has not been performed yet in this context. Furthermore, the presence of the LMA-D solution in presence of NSI with electrons remains an open question.

In this work we address these open issues by updating and extending our analyses in refs. [29, 47] accounting for the possibility of NC NSI with up quarks, down quarks and electrons *simultaneously*. We will consider vector and axial-vector couplings separately. Our global analysis updates that of our previous works, with the major addition of the Borexino Phase-II spectral dataset. Furthermore when combining with $CE\nu NS$ we include the results from COHERENT data on CsI [46, 48] and Ar targets [49, 55] together with the recent results from $CE\nu NS$ searches using reactor neutrinos at Dresden-II reactor experiment [52, 56]. To this aim, in section 2 we briefly summarize the framework of our study. We present the main ingredients and assumptions in the analysis of the NSI effects in the matter potential in atmospheric and long-baseline (LBL) experiments in section 2.1.1, and Solar and KamLAND in section 2.1.2. In particular, we include a discussion on the possible departures from adiabaticity of the evolution of solar neutrinos in section 2.1.3. The effects of NC NSI on the detection cross sections and its interplay with flavour transitions in propagation is reviewed in section 2.2 including the specific modification of the cross section for ES (section 2.2.1), NC scattering with quarks (section 2.2.2), and $CE\nu NS$ (section 2.2.3). The results of the different analyses performed are presented in section 3 where we derive

our current knowledge of the size and flavour structure of vector NC NSI coupling to either electrons (section 3.2), up and down quarks (section 3.3), or a general combination of those (section 3.4). We study the status of the LMA-D solution as function of the relative strength of the non-standard couplings to the different charged fermions in section 3.5. We also quantify the results as allowed ranges of the effective combinations of couplings relevant for long-baseline and atmospheric oscillation experiments. In section 4 we summarize our conclusions.

2 Formalism

As stated in the introduction, in this work we will consider NC NSI (hereafter referred to simply as NSI, for brevity) relevant to neutrino scattering and propagation in matter, as parametrized in eq. (1.2). To make the analysis feasible, the following simplifications are introduced:

- we assume that the neutrino flavour structure of the interactions is independent of the charged fermion properties;
- we further assume that the chiral structure of the charged fermion vertex is the same for all fermion types.

Under these hypotheses, we can factorize $\varepsilon_{\alpha\beta}^{f,P}$ as the product of three terms:

$$\varepsilon_{\alpha\beta}^{f,P} \equiv \varepsilon_{\alpha\beta} \xi^f \chi^P \tag{2.1}$$

where the matrix $\varepsilon_{\alpha\beta}$ describes the dependence on the neutrino flavour, the coefficients ξ^f parametrize the coupling to the charged fermions, and the terms χ^P account for the chiral structure of such couplings, normalized so that $\varepsilon_{\alpha\beta}^{f,L}$ ($\varepsilon_{\alpha\beta}^{f,R}$) corresponds to $\chi^L = 1/2$ and $\chi^R = 0$ ($\chi^R = 1/2$ and $\chi^L = 0$). With these assumptions the Lagrangian in eq. (1.2) takes the form:

$$\mathcal{L}_{\text{NSI,NC}} = -2\sqrt{2}G_F \left[\sum_{\alpha,\beta} \varepsilon_{\alpha\beta} (\bar{\nu}_\alpha \gamma^\mu P_L \nu_\beta) \right] \left[\sum_{f,P} \xi^f \chi^P (\bar{f} \gamma_\mu P f) \right]. \tag{2.2}$$

Concerning the chiral structure of the charged fermion vertex, in this work we will consider either vector couplings ($\chi^L = \chi^R = 1/2$), or axial-vector couplings ($\chi^L = -\chi^R = 1/2$). The corresponding combinations of NSI coefficients are given in eq. (1.3).

For what concerns the dependence of the NSI on the charged fermion type, we notice that ordinary matter is composed of electrons (e), up quarks (u) and down quarks (d), so that only the coefficients ξ^e , ξ^u and ξ^d are experimentally accessible. For vector NSI, since quarks are always confined inside protons (p) and neutrons (n), we may define (see, e.g., ref. [5]):

$$\xi^p = 2\xi^u + \xi^d, \quad \xi^n = 2\xi^d + \xi^u \tag{2.3}$$

so that $\varepsilon_{\alpha\beta}^{p,V} \equiv 2\varepsilon_{\alpha\beta}^{u,V} + \varepsilon_{\alpha\beta}^{d,V} = \varepsilon_{\alpha\beta} \xi^p (\chi^L + \chi^R)$ and $\varepsilon_{\alpha\beta}^{n,V} \equiv 2\varepsilon_{\alpha\beta}^{d,V} + \varepsilon_{\alpha\beta}^{u,V} = \varepsilon_{\alpha\beta} \xi^n (\chi^L + \chi^R)$. For axial-vector NSI, the correspondence between quark NSI and nucleon NSI is not that obvious: for example, for non-relativistic nucleons an axial-vector hadronic current would

induce a change in the spin of the nucleon. In our analysis this type of NSI is only relevant for the breakup of deuterium at SNO as discussed in section 2.2.2. In any case, it is clear that a simultaneous re-scaling of all $\{\xi^f\}$ by a common factor can be reabsorbed into a re-scaling of $\varepsilon_{\alpha\beta}$, so that only the direction of (ξ^e, ξ^u, ξ^d) — or, equivalently, (ξ^e, ξ^p, ξ^n) — is phenomenologically non-trivial. We parametrize such direction using spherical coordinates, in terms of a “latitude” angle η and a “longitude” angle ζ , as an extension of the framework and notation introduced in ref. [29] (see also ref. [57]). Concretely, we define:

$$\xi^e = \sqrt{5} \cos \eta \sin \zeta, \quad \xi^p = \sqrt{5} \cos \eta \cos \zeta, \quad \xi^n = \sqrt{5} \sin \eta \quad (2.4)$$

or, in terms of the “quark” couplings:

$$\xi^u = \frac{\sqrt{5}}{3} (2 \cos \eta \cos \zeta - \sin \eta), \quad \xi^d = \frac{\sqrt{5}}{3} (2 \sin \eta - \cos \eta \cos \zeta) \quad (2.5)$$

Using this parametrization, the case of NSI with quarks analyzed in ref. [29] correspond to the “prime meridian” $\zeta = 0$, with the pure up-quark and pure down-quark cases located at $\eta = \arctan(1/2) \approx 26.6^\circ$ and $\eta = \arctan(2) \approx 63.4^\circ$, respectively. The “poles” ($\eta = \pm 90^\circ$) correspond to NSI with neutrons, while NSI with protons lies on the “equator” ($\eta = \zeta = 0$). Finally, the pure electron case is also on the equator, at a right angle ($\zeta = \pm 90^\circ$) from the pure proton case. Notice that an overall sign flip of (ξ^e, ξ^u, ξ^d) is just a special case of re-scaling and produces no observable effect, hence it is sufficient to restrict both η and ζ to the $[-90^\circ, +90^\circ]$ range.

The presence of vector NC NSI will affect both neutrino propagation in matter and neutrino scattering in the detector, while axial-vector NC NSI only affect some of the interaction cross sections. Both propagation and interaction effects lead to a modification of the expected number of events which can be described by the generic expression [54]:

$$N_{\text{ev}} \propto \text{Tr} \left[\rho^{\text{det}} \sigma^{\text{det}} \right] \quad (2.6)$$

where ρ^{det} is the density matrix characterizing the flavour state of the neutrinos reaching the detector, while the *generalized* cross section σ^{det} is a matrix in flavour space containing enough information to describe the interaction of *any* neutrino configuration. The form of eq. (2.6) is manifestly basis-independent and permits a separate description of propagation effects (encoded into ρ^{det}) and of the scattering process (contained in σ^{det}), while at the same time properly taking into account possible interference between them. Notice that both ρ^{det} and σ^{det} are hermitian matrices, which ensures that N_{ev} is real. Actually, eq. (2.6) is invariant under the joint transformation:

$$\rho^{\text{det}} \rightarrow [\rho^{\text{det}}]^* \quad \text{and} \quad \sigma^{\text{det}} \rightarrow [\sigma^{\text{det}}]^* \quad (2.7)$$

whose implications will be discussed later on in this section.

2.1 Neutrino oscillations in the presence of NSI

In general, the evolution of the neutrino and antineutrino flavour state during propagation is governed by the Hamiltonian:

$$H^\nu = H_{\text{vac}} + H_{\text{mat}} \quad \text{and} \quad H^{\bar{\nu}} = (H_{\text{vac}} - H_{\text{mat}})^*, \quad (2.8)$$

where H_{vac} is the vacuum part which in the flavour basis $(\nu_e, \nu_\mu, \nu_\tau)$ reads

$$H_{\text{vac}} = U_{\text{vac}} D_{\text{vac}} U_{\text{vac}}^\dagger \quad \text{with} \quad D_{\text{vac}} = \frac{1}{2E_\nu} \text{diag}(0, \Delta m_{21}^2, \Delta m_{31}^2). \quad (2.9)$$

Here U_{vac} denotes the three-lepton mixing matrix in vacuum [1, 58, 59]. Following the convention of ref. [35], we define $U_{\text{vac}} = R_{23}(\theta_{23})R_{13}(\theta_{13})\tilde{R}_{12}(\theta_{12}, \delta_{\text{CP}})$, where $R_{ij}(\theta_{ij})$ is a rotation of angle θ_{ij} in the ij plane and $\tilde{R}_{12}(\theta_{12}, \delta_{\text{CP}})$ is a complex rotation by angle θ_{12} and phase δ_{CP} . Explicitly:

$$U_{\text{vac}} = \begin{pmatrix} c_{12}c_{13} & s_{12}c_{13}e^{i\delta_{\text{CP}}} & s_{13} \\ -s_{12}c_{23}e^{-i\delta_{\text{CP}}} - c_{12}s_{13}s_{23} & c_{12}c_{23} - s_{12}s_{13}s_{23}e^{i\delta_{\text{CP}}} & c_{13}s_{23} \\ s_{12}s_{23}e^{-i\delta_{\text{CP}}} - c_{12}s_{13}c_{23} & -c_{12}s_{23} - s_{12}s_{13}c_{23}e^{i\delta_{\text{CP}}} & c_{13}c_{23} \end{pmatrix} \quad (2.10)$$

where $c_{ij} \equiv \cos \theta_{ij}$ and $s_{ij} \equiv \sin \theta_{ij}$. This expression differs from the usual one “ U ” (defined, e.g., in eq. (1.1) of ref. [60]) by an overall phase matrix: $U_{\text{vac}} = PUP^*$ with $P = \text{diag}(e^{i\delta_{\text{CP}}}, 1, 1)$. It is easy to show that, in the absence of NSI, such rephasing produces no visible effect, so that when only standard interactions are considered the physical interpretation of the vacuum parameters ($\Delta m_{21}^2, \Delta m_{31}^2, \theta_{12}, \theta_{13}, \theta_{23}$ and δ_{CP}) is exactly the same in both conventions. The advantage of defining U_{vac} as in eq. (2.10) is that the transformation $H_{\text{vac}} \rightarrow -H_{\text{vac}}^*$, whose relevance for the present work will be discussed below, can be implemented exactly (up to an irrelevant multiple of the identity) by the following transformation of the parameters:

$$\begin{aligned} \Delta m_{31}^2 &\rightarrow -\Delta m_{31}^2 + \Delta m_{21}^2 = -\Delta m_{32}^2, \\ \theta_{12} &\rightarrow \pi/2 - \theta_{12}, \\ \delta_{\text{CP}} &\rightarrow \pi - \delta_{\text{CP}} \end{aligned} \quad (2.11)$$

which does not spoil the commonly assumed restrictions on the range of the vacuum parameters ($\Delta m_{21}^2 > 0$ and $0 \leq \theta_{ij} \leq \pi/2$).

Concerning the matter part H_{mat} of the Hamiltonian which governs neutrino oscillations, if all possible operators in eq. (1.2) are added to the SM Lagrangian we get:

$$H_{\text{mat}} = \sqrt{2}G_F N_e(x) \begin{pmatrix} 1 + \mathcal{E}_{ee}(x) & \mathcal{E}_{e\mu}(x) & \mathcal{E}_{e\tau}(x) \\ \mathcal{E}_{e\mu}^*(x) & \mathcal{E}_{\mu\mu}(x) & \mathcal{E}_{\mu\tau}(x) \\ \mathcal{E}_{e\tau}^*(x) & \mathcal{E}_{\mu\tau}^*(x) & \mathcal{E}_{\tau\tau}(x) \end{pmatrix} \quad (2.12)$$

where the “+1” term in the ee entry accounts for the standard contribution, and

$$\mathcal{E}_{\alpha\beta}(x) = \sum_{f=e,u,d} \frac{N_f(x)}{N_e(x)} \varepsilon_{\alpha\beta}^{f,V} \quad (2.13)$$

describes the non-standard part. Here $N_f(x)$ is the number density of fermion f as a function of the distance traveled by the neutrino along its trajectory. In eq. (2.13) we have limited the sum to the charged fermions present in ordinary matter, $f = e, u, d$. Taking into account that $N_u(x) = 2N_p(x) + N_n(x)$ and $N_d(x) = N_p(x) + 2N_n(x)$, and also that matter neutrality implies $N_p(x) = N_e(x)$, eq. (2.13) becomes:

$$\mathcal{E}_{\alpha\beta}(x) = (\varepsilon_{\alpha\beta}^{e,V} + \varepsilon_{\alpha\beta}^{p,V}) + Y_n(x) \varepsilon_{\alpha\beta}^{n,V} \quad \text{with} \quad Y_n(x) \equiv \frac{N_n(x)}{N_e(x)} \quad (2.14)$$

which shows that, from the phenomenological point of view, the propagation effects of NSI with electrons can be mimicked by NSI with quarks by means of a suitable combination of up-quark and down-quark contributions.

Since the matter potential can be determined by oscillation experiments only up to an overall multiple of the identity, each $\varepsilon_{\alpha\beta}^{f,V}$ matrix introduces 8 new parameters: two differences of the three diagonal real parameters (e.g., $\varepsilon_{ee}^{f,V} - \varepsilon_{\mu\mu}^{f,V}$ and $\varepsilon_{\tau\tau}^{f,V} - \varepsilon_{\mu\mu}^{f,V}$) and three off-diagonal complex parameters (i.e., three additional moduli and three complex phases). Under the assumption that the neutrino flavour structure of the interactions is independent of the charged fermion type, as described in eq. (2.1), we get:

$$\begin{aligned} \mathcal{E}_{\alpha\beta}(x) &= \varepsilon_{\alpha\beta} [\xi^e + \xi^p + Y_n(x)\xi^n] (\chi^L + \chi^R) \\ &= \sqrt{5} [\cos \eta (\cos \zeta + \sin \zeta) + Y_n(x) \sin \eta] (\chi^L + \chi^R) \varepsilon_{\alpha\beta} \end{aligned} \quad (2.15)$$

so that the phenomenological framework adopted here is characterized by 10 matter parameters: eight related to the matrix $\varepsilon_{\alpha\beta}$ plus two directions (η, ζ) in the (ξ^e, ξ^p, ξ^n) space. Notice, however, that the dependence on ζ in eq. (2.15) can be reabsorbed into a re-scaling of $\varepsilon_{\alpha\beta}$ by introducing a new effective angle η' :

$$\begin{aligned} \mathcal{E}_{\alpha\beta}(x) &= \sqrt{5} [\cos \eta' + Y_n(x) \sin \eta'] (\chi^L + \chi^R) \varepsilon'_{\alpha\beta} \\ \text{with } \tan \eta' &\equiv \tan \eta / (\cos \zeta + \sin \zeta) \quad \text{and} \quad \varepsilon'_{\alpha\beta} \equiv \varepsilon_{\alpha\beta} \sqrt{1 + \cos^2 \eta \sin(2\zeta)}. \end{aligned} \quad (2.16)$$

This is a consequence of the fact that electron and proton NSI always appear together in propagation, as explained after eq. (2.14). Indeed, η' is just a practical way to express the direction in the $(\xi^e + \xi^p, \xi^n)$ plane. For $\zeta = 0$, which is the case studied in ref. [29], one trivially recovers $\eta' = \eta$ and $\varepsilon'_{\alpha\beta} = \varepsilon_{\alpha\beta}$. Furthermore, for $\zeta = -45^\circ$ one gets $\xi^e + \xi^p = 0$, so that NSI effects in oscillations depend solely on the neutron coupling ξ^n . This would be the case, for example, in models where the Z' does not couple directly to matter fermions, and NSI are generated through $Z - Z'$ mass mixing (see the related discussion in ref. [19]). In fact, in this case, the specific value of η becomes irrelevant as long as it is different from zero (since eq. (2.16) always yields $\eta' = \pm 90^\circ$ in this case), while for the special point where $\eta = 0$ and $\zeta = -45^\circ$ NSI completely cancel from oscillations. It should be stressed, however, that this only applies to *oscillations*: the implications of NSI for neutrino scattering described in section 2.2 will still depend non-trivially on η .

We finish this section by reminding that the neutrino transition probabilities remain invariant — and more generically the density matrix ρ^{det} undergoes complex conjugation, as described in eq. (2.7) — if the Hamiltonian $H^\nu = H_{\text{vac}} + H_{\text{mat}}$ is transformed as $H^\nu \rightarrow -(H^\nu)^*$. This requires a simultaneous transformation of both the vacuum and the matter terms. The transformation of H_{vac} is described in eq. (2.11) and involves a change in the octant of θ_{12} (the so-called LMA-D [32] solution) as well as a change in the neutrino mass ordering (i.e., the sign of Δm_{31}^2), which is why it has been called “generalized mass-ordering degeneracy” in ref. [35]. As for H_{mat} we need:

$$\begin{aligned} [\mathcal{E}_{ee}(x) - \mathcal{E}_{\mu\mu}(x)] &\rightarrow -[\mathcal{E}_{ee}(x) - \mathcal{E}_{\mu\mu}(x)] - 2, \\ [\mathcal{E}_{\tau\tau}(x) - \mathcal{E}_{\mu\mu}(x)] &\rightarrow -[\mathcal{E}_{\tau\tau}(x) - \mathcal{E}_{\mu\mu}(x)], \\ \mathcal{E}_{\alpha\beta}(x) &\rightarrow -\mathcal{E}_{\alpha\beta}^*(x) \quad (\alpha \neq \beta), \end{aligned} \quad (2.17)$$

see refs. [28, 34, 35]. As seen in eqs. (2.13), (2.14) and (2.15) the matrix $\mathcal{E}_{\alpha\beta}(x)$ depends on the chemical composition of the medium, which may vary along the neutrino trajectory, so that in general the condition in eq. (2.17) is fulfilled only in an approximate way. The degeneracy becomes exact in the following two cases:¹

- if the effective NSI coupling to neutrons vanishes, so that $\varepsilon_{\alpha\beta}^{n,V} = 0$ in eq. (2.14). In terms of fundamental quantities this occurs when $\varepsilon_{\alpha\beta}^{u,V} = -2\varepsilon_{\alpha\beta}^{d,V}$, i.e., the NSI couplings are proportional to the electric charge of quarks. In our parametrization this corresponds to the “equator” $\eta = 0$ for arbitrary ζ , as shown in eq. (2.15);
- if the neutron/proton ratio $Y_n(x)$ is constant along the entire neutrino propagation path. This is certainly the case for reactor and long-baseline experiments, where only the Earth’s mantle is involved, and to a good approximation also for atmospheric neutrinos, since the differences in chemical composition between mantle and core can safely be neglected in the context of NSI [33]. In this case the matrix $\mathcal{E}_{\alpha\beta}(x)$ becomes independent of x and can be regarded as a new phenomenological parameter, as we will describe in section 2.1.1.

Further details on the implications of this degeneracy for different classes of neutrino experiments (solar, atmospheric, etc.) is provided below in the corresponding section.

2.1.1 Matter potential in atmospheric and long-baseline neutrinos

As discussed in ref. [33], in the Earth the neutron/proton ratio $Y_n(x)$ which characterizes the matter chemical composition can be taken to be constant to very good approximation. The PREM model [61] fixes $Y_n = 1.012$ in the Mantle and $Y_n = 1.137$ in the Core, with an average value $Y_n^\oplus = 1.051$ all over the Earth. Setting therefore $Y_n(x) \equiv Y_n^\oplus$ in eqs. (2.13) and (2.14) we get $\mathcal{E}_{\alpha\beta}(x) \equiv \varepsilon_{\alpha\beta}^\oplus$ with:

$$\varepsilon_{\alpha\beta}^\oplus = \varepsilon_{\alpha\beta}^{e,V} + (2 + Y_n^\oplus)\varepsilon_{\alpha\beta}^{u,V} + (1 + 2Y_n^\oplus)\varepsilon_{\alpha\beta}^{d,V} = (\varepsilon_{\alpha\beta}^{e,V} + \varepsilon_{\alpha\beta}^{p,V}) + Y_n^\oplus\varepsilon_{\alpha\beta}^{n,V}. \quad (2.18)$$

If we impose quark-lepton factorization as in eq. (2.15) we get:

$$\begin{aligned} \varepsilon_{\alpha\beta}^\oplus &= \sqrt{5} [\cos \eta (\cos \zeta + \sin \zeta) + Y_n^\oplus \sin \eta] (\chi^L + \chi^R) \varepsilon_{\alpha\beta} \\ &= \sqrt{5} [\cos \eta' + Y_n^\oplus \sin \eta'] (\chi^L + \chi^R) \varepsilon'_{\alpha\beta}. \end{aligned} \quad (2.19)$$

In other words, within this approximation the analysis of atmospheric and LBL neutrinos holds for any combination of NSI with up, down or electrons and it can be performed in terms of the effective NSI couplings $\varepsilon_{\alpha\beta}^\oplus$, which play the role of phenomenological parameters. In particular, the best-fit value and allowed ranges of $\varepsilon_{\alpha\beta}^\oplus$ are independent of η and ζ , while the bounds on $\varepsilon_{\alpha\beta}$ simply scale as $[\cos \eta (\cos \zeta + \sin \zeta) + Y_n^\oplus \sin \eta]$. Moreover, it is immediate to see that for $\eta' = \arctan(-1/Y_n^\oplus) \approx -43.6^\circ$, with η' defined in eq. (2.16), the contribution of NSI to the matter potential vanishes, so that no bound on $\varepsilon_{\alpha\beta}$ can be derived from

¹Strictly speaking, eq. (2.17) can be satisfied exactly for *any* matter chemical profile $Y_n(x)$ if $\varepsilon_{\alpha\beta}^{n,V}$ and $\varepsilon_{\alpha\beta}^{e,V} + \varepsilon_{\alpha\beta}^{p,V}$ are allowed to transform independently of each other. This possibility, however, is incompatible with the factorization constraint of eq. (2.1), so it will not be discussed here.

atmospheric and LBL data in such case. This would be approximately the case, for example, for $U(1)'$ models associated to the combination $B - 2L_e + \alpha L_\mu - \beta L_\tau$ and, consequently, oscillation bounds are significantly relaxed for this type of models [18].

Following the approach of ref. [33], the matter Hamiltonian H_{mat} , given in eq. (2.12) after setting $\mathcal{E}_{\alpha\beta}(x) \equiv \varepsilon_{\alpha\beta}^\oplus$, can be parametrized in a way that mimics the structure of the vacuum term (2.9):

$$H_{\text{mat}} = Q_{\text{rel}} U_{\text{mat}} D_{\text{mat}} U_{\text{mat}}^\dagger Q_{\text{rel}}^\dagger \quad \text{with} \quad \begin{cases} Q_{\text{rel}} = \text{diag} \left(e^{i\alpha_1}, e^{i\alpha_2}, e^{-i\alpha_1 - i\alpha_2} \right), \\ U_{\text{mat}} = R_{12}(\varphi_{12}) R_{13}(\varphi_{13}) \tilde{R}_{23}(\varphi_{23}, \delta_{\text{NS}}), \\ D_{\text{mat}} = \sqrt{2} G_F N_e(x) \text{diag}(\varepsilon_\oplus, \varepsilon'_\oplus, 0) \end{cases} \quad (2.20)$$

where $R_{ij}(\varphi_{ij})$ is a rotation of angle φ_{ij} in the ij plane and $\tilde{R}_{23}(\varphi_{23}, \delta_{\text{NS}})$ is a complex rotation by angle φ_{23} and phase δ_{NS} . Note that the two phases α_1 and α_2 included in Q_{rel} are not a feature of neutrino-matter interactions, but rather a relative feature of the vacuum and matter terms. In order to simplify the analysis we impose that two eigenvalues of H_{mat} are equal, $\varepsilon'_\oplus = 0$. This assumption is justified since, as shown in ref. [62], in this case strong cancellations in the oscillation of atmospheric neutrinos occur, and this is precisely the situation in which the weakest constraints can be placed. Setting $\varepsilon'_\oplus \rightarrow 0$ implies that the φ_{23} angle and the δ_{NS} phase disappear from neutrino oscillations, so that the effective NSI couplings $\varepsilon_{\alpha\beta}^\oplus$ can be parametrized as:

$$\begin{aligned} \varepsilon_{ee}^\oplus - \varepsilon_{\mu\mu}^\oplus &= \varepsilon_\oplus (\cos^2 \varphi_{12} - \sin^2 \varphi_{12}) \cos^2 \varphi_{13} - 1, \\ \varepsilon_{\tau\tau}^\oplus - \varepsilon_{\mu\mu}^\oplus &= \varepsilon_\oplus (\sin^2 \varphi_{13} - \sin^2 \varphi_{12} \cos^2 \varphi_{13}), \\ \varepsilon_{e\mu}^\oplus &= -\varepsilon_\oplus \cos \varphi_{12} \sin \varphi_{12} \cos^2 \varphi_{13} e^{i(\alpha_1 - \alpha_2)}, \\ \varepsilon_{e\tau}^\oplus &= -\varepsilon_\oplus \cos \varphi_{12} \cos \varphi_{13} \sin \varphi_{13} e^{i(2\alpha_1 + \alpha_2)}, \\ \varepsilon_{\mu\tau}^\oplus &= \varepsilon_\oplus \sin \varphi_{12} \cos \varphi_{13} \sin \varphi_{13} e^{i(\alpha_1 + 2\alpha_2)}. \end{aligned} \quad (2.21)$$

As further simplification, in order to keep the fit manageable we assume real NSI, which we implement by choosing $\alpha_1 = \alpha_2 = 0$ and $-\pi/2 \leq \varphi_{ij} \leq \pi/2$, and also restrict $\delta_{\text{CP}} \in \{0, \pi\}$. It is important to note that with these approximations the formalism for atmospheric and long-baseline data is CP-conserving; we will go back to this point when discussing the experimental results included in the fit. In addition to atmospheric and LBL experiments, important information on neutrino oscillation parameters is provided also by reactor experiments with a baseline of about 1 km. Due to the very small amount of matter crossed, both standard and non-standard matter effects are completely irrelevant for these experiments, so that neutrino propagation depends only on the vacuum parameters.

2.1.2 Matter potential for solar and KamLAND neutrinos

For the study of propagation of solar and KamLAND neutrinos one can work in the one mass dominance approximation, $\Delta m_{31}^2 \rightarrow \infty$ (which effectively means that $G_F \sum_f N_f(x) \varepsilon_{\alpha\beta}^{f,V} \ll \Delta m_{31}^2/E_\nu$). In this limit the neutrino evolution can be calculated in an effective 2×2 model

described by the Hamiltonian $H_{\text{eff}} = H_{\text{vac}}^{\text{eff}} + H_{\text{mat}}^{\text{eff}}$, with:

$$H_{\text{vac}}^{\text{eff}} = \frac{\Delta m_{21}^2}{4E_\nu} \begin{pmatrix} -\cos 2\theta_{12} & \sin 2\theta_{12} e^{i\delta_{\text{CP}}} \\ \sin 2\theta_{12} e^{-i\delta_{\text{CP}}} & \cos 2\theta_{12} \end{pmatrix}, \quad (2.22)$$

$$H_{\text{mat}}^{\text{eff}} = \sqrt{2}G_F N_e(x) \left[\frac{c_{13}^2}{2} \begin{pmatrix} 1 & 0 \\ 0 & -1 \end{pmatrix} + [\xi^e + \xi^p + Y_n(x)\xi^n](\chi^L + \chi^R) \begin{pmatrix} -\varepsilon_D & \varepsilon_N \\ \varepsilon_N^* & \varepsilon_D \end{pmatrix} \right], \quad (2.23)$$

where we have imposed the quark-lepton factorization of eq. (2.15) and used the parametrization convention of eq. (2.10) for U_{vac} . The coefficients ε_D and ε_N are related to the original parameters $\varepsilon_{\alpha\beta}$ by the following relations:

$$\begin{aligned} \varepsilon_D &= c_{13}s_{13} \text{Re}(s_{23}\varepsilon_{e\mu} + c_{23}\varepsilon_{e\tau}) - (1 + s_{13}^2)c_{23}s_{23} \text{Re}(\varepsilon_{\mu\tau}) \\ &\quad - \frac{c_{13}^2}{2}(\varepsilon_{ee} - \varepsilon_{\mu\mu}) + \frac{s_{23}^2 - s_{13}^2 c_{23}^2}{2}(\varepsilon_{\tau\tau} - \varepsilon_{\mu\mu}), \end{aligned} \quad (2.24)$$

$$\varepsilon_N = c_{13}(c_{23}\varepsilon_{e\mu} - s_{23}\varepsilon_{e\tau}) + s_{13} \left[s_{23}^2\varepsilon_{\mu\tau} - c_{23}^2\varepsilon_{\mu\tau}^* + c_{23}s_{23}(\varepsilon_{\tau\tau} - \varepsilon_{\mu\mu}) \right]. \quad (2.25)$$

Denoting by S_{eff} the 2×2 unitary matrix obtained integrating H_{eff} along the neutrino trajectory, the full density matrix ρ^{det} introduced in eq. (2.6) can be written as:

$$\rho_{\alpha\beta}^{\text{det}} = c_{13}^2 [A_{\alpha\beta}P_{\text{osc}} + B_{\alpha\beta}P_{\text{int}} + iC_{\alpha\beta}P_{\text{ext}}] + D_{\alpha\beta} \quad (2.26)$$

where the effective probabilities P_{osc} , P_{int} and P_{ext} are given by

$$P_{\text{osc}} \equiv |S_{21}^{\text{eff}}|^2, \quad P_{\text{int}} \equiv \text{Re}(S_{11}^{\text{eff}}S_{21}^{\text{eff}*}), \quad P_{\text{ext}} \equiv \text{Im}(S_{11}^{\text{eff}}S_{21}^{\text{eff}*}), \quad (2.27)$$

and the numerical coefficients $A_{\alpha\beta}$, $B_{\alpha\beta}$, $C_{\alpha\beta}$ and $D_{\alpha\beta}$ are defined as

$$\begin{aligned} A_{\alpha\beta} &\equiv O_{\alpha 2}O_{\beta 2} - O_{\alpha 1}O_{\beta 1}, & B_{\alpha\beta} &\equiv O_{\alpha 1}O_{\beta 2} + O_{\alpha 2}O_{\beta 1}, \\ C_{\alpha\beta} &\equiv O_{\alpha 1}O_{\beta 2} - O_{\alpha 2}O_{\beta 1}, & D_{\alpha\beta} &\equiv \sum_{i=\text{all}} O_{\alpha i}O_{\beta i}|O_{ei}|^2. \end{aligned} \quad (2.28)$$

with $O = R_{23}(\theta_{23})R_{13}(\theta_{13})$. Unlike in ref. [29] where NSI did *not* affect the scattering process and only the ρ_{ee}^{det} entry (which depends exclusively on P_{osc}) was required, a rephasing of S_{eff} now produces visible consequences as it affects P_{int} and P_{ext} . Moreover, ν_μ and ν_τ are no longer indistinguishable as their scattering amplitude may be different under NSI, so that the θ_{23} angle acquires relevance. Hence, for each fixed value of η and ζ the density matrix ρ^{det} for solar and KamLAND neutrinos depends effectively on eight quantities: the four real oscillation parameters θ_{12} , θ_{13} , θ_{23} and Δm_{21}^2 , the real ε_D and complex ε_N matter parameters, and the CP phase δ_{CP} . As stated in section 2.1.1 in this work we will assume real NSI, implemented here by setting $\delta_{\text{CP}} \in \{0, \pi\}$ and considering only real values for ε_N .

Unlike in the Earth, the matter chemical composition of the Sun varies substantially along the neutrino trajectory, and consequently the potential depends non-trivially on the specific combinations of $(\xi^e + \xi^p)$ and ξ^n couplings — i.e., on the value of η' as determined by the (η, ζ) parameters. This implies that the generalized mass-ordering degeneracy is not exact, except for $\eta = 0$ (in which case the NSI potential is proportional to the standard MSW potential and an exact inversion of the matter sign is possible). However the transformation described in eqs. (2.11) and (2.17) still results in a good fit to the global analysis of oscillation data for a wide range of values of η' , and non-oscillation data are needed to break this degeneracy [35].

2.1.3 Departures from adiabaticity in presence of NSI

When computing neutrino evolution in the Sun, it is often assumed that it takes place in the adiabatic regime, as this considerably simplifies the calculation. While this is the case for neutrino oscillations within the LMA solution with a standard matter potential, it is worthwhile asking if the inclusion of NP effects (such as NSI) can lead to non-adiabatic transitions. If this were the case, it would require special care and may lead to interesting new phenomenological consequences. This possibility has been largely overlooked in the literature, where most studies of NSI in the Sun assume adiabatic transitions.

Let us consider the two-neutrino case, with a matter potential that depends on the position x along the neutrino path inside the Sun. In the instantaneous mass basis, the Hamiltonian can be written as:

$$i \frac{d}{dx} \begin{pmatrix} \tilde{\nu}_1 \\ \tilde{\nu}_2 \end{pmatrix} = \begin{pmatrix} -\Delta_m(x) & -i\theta'_m(x) \\ i\theta'_m(x) & \Delta_m(x) \end{pmatrix} \begin{pmatrix} \tilde{\nu}_1 \\ \tilde{\nu}_2 \end{pmatrix} \quad (2.29)$$

where $\theta_m(x)$ and $\Delta_m(x)$ refer to the mixing angle and oscillation frequency in the presence of matter effects, and $\theta'(x) \equiv d\theta(x)/dx$. In this basis, transitions between $\tilde{\nu}_1 \leftrightarrow \tilde{\nu}_2$ are negligible as long as the off-diagonal terms $\theta'_m(x)$ are small compared to the diagonal entries $\Delta_m(x)$ in eq. (2.29). This leads to the so-called adiabaticity condition, that is:

$$\gamma^{-1}(x) \equiv \left| \frac{\theta'_m(x)}{\Delta_m(x)} \right| \ll 1. \quad (2.30)$$

Neutrino transitions will be adiabatic if this condition is satisfied along all points in the neutrino trajectory. Of course, this argument is general and may be applied both in the standard case and in the presence of NP. In the present work neutrino propagation is described by the effective 2×2 Hamiltonian H_{eff} introduced in eqs. (2.22) and (2.23). Assuming $\delta_{\text{CP}} = 0$ and real NSI, so that H_{eff} is traceless and real with $H_{11}^{\text{eff}} = -H_{22}^{\text{eff}}$ and $H_{12}^{\text{eff}} = H_{21}^{\text{eff}}$, we can write:

$$\theta_m(x) \equiv \frac{1}{2} \arctan[H_{12}^{\text{eff}}(x) / H_{22}^{\text{eff}}(x)] \quad \text{and} \quad \Delta_m(x) \equiv \sqrt{[H_{12}^{\text{eff}}(x)]^2 + [H_{22}^{\text{eff}}(x)]^2}. \quad (2.31)$$

In the presence of NSI, for a given matter density and neutrino energy, it is possible to choose ε_D and ε_N so that the contribution from NP cancels the standard one, resulting in $\Delta_m(x) \rightarrow 0$. It is easy to show analytically that, for such values, the adiabatic condition in eq. (2.30) is no longer satisfied. Specifically, such cancellation takes place when:

$$\begin{aligned} [\xi^e + \xi^p + Y_n(x)\xi^n](\chi^L + \chi^R) \varepsilon_D &\rightarrow -\frac{\Delta m_{12}^2 \cos 2\theta_{12}}{4E_\nu V(x)} + \frac{c_{13}^2}{2}, \\ [\xi^e + \xi^p + Y_n(x)\xi^n](\chi^L + \chi^R) \varepsilon_N &\rightarrow -\frac{\Delta m_{12}^2 \sin 2\theta_{12}}{4E_\nu V(x)}, \end{aligned} \quad (2.32)$$

where $V(x) \equiv \sqrt{2}G_F N_e(x)$ is the SM matter potential. In other words, for a neutrino with a given energy E_ν at some point x along the trajectory, it is possible to find a pair of values $(\varepsilon_D, \varepsilon_N)$ for which transitions are no longer adiabatic. Note that the cancellation condition for ε_D depends on $\cos 2\theta_{12}$ and therefore will take different values for the LMA

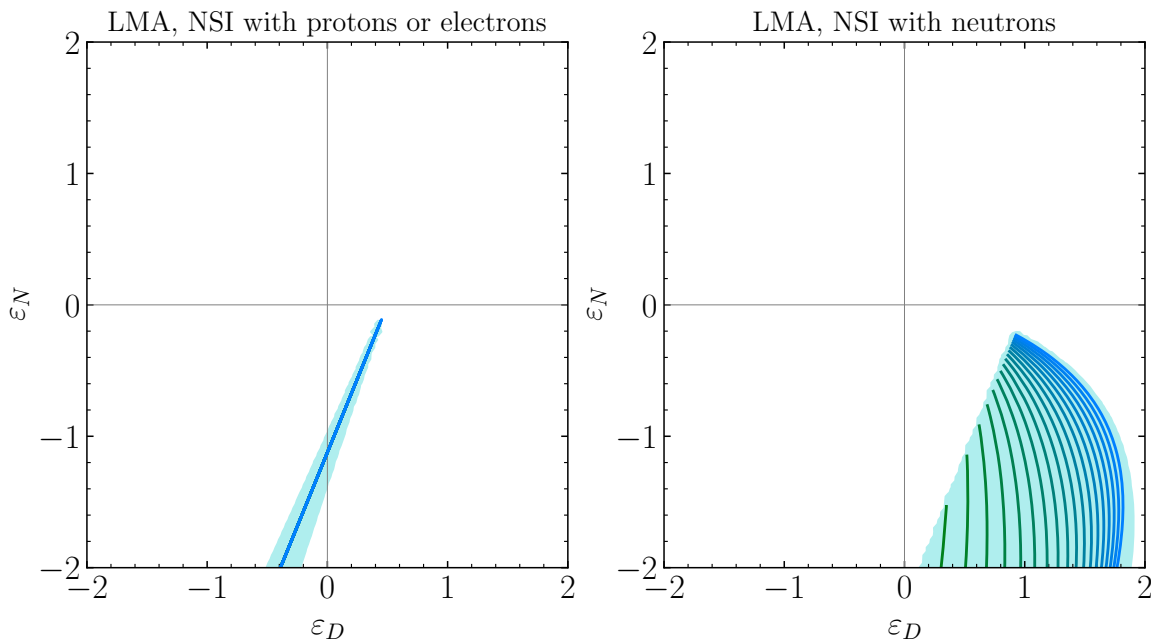


Figure 1. Departure from the adiabatic regime in presence of NSI, for a solar mixing angle in the LMA region. The pale blue regions show the values of NSI parameters leading to $\gamma^{-1} > 1$, obtained from a numerical computation. The coloured lines show the values of NSI parameters where eqs. (2.32) are satisfied at some point along the neutrino trajectory, for a neutrino produced at the center of the Sun. The different lines in the right panel correspond to neutrino energies between 1 MeV (green lines, at the left edge of the region) and 20 MeV (blue lines, towards the right edge).

and LMA-D regions, while the corresponding value for ε_N will remain invariant under a change of octant for θ_{12} . Also, as the cancellation conditions in eqs. (2.32) depend on the values of ξ^f , the regions will depend on whether NSI take place with electrons/protons, neutrons, or a combination of the two.

Figure 1 shows the regions where the transitions are not adiabatic, for NSI with protons or electrons (left panel) and for NSI with neutrons (right panel). The shaded pale blue regions show the results from a numerical computation. In contrast, the coloured lines show the points satisfying the analytic conditions in eqs. (2.32), for neutrino energies between 1 MeV (green lines, towards the left edge of the region) and 20 MeV (blue lines, towards the right edge of the region), for $\theta_{12} = 33^\circ$ and $\Delta m_{12}^2 = 7.5 \times 10^{-5} \text{ eV}^2$. As can be seen, the agreement with the numerical computation is excellent. Also, note the very different shape of the regions in the two panels. The reason behind this is that for NSI with electrons or protons the dependence with E_ν and x comes in eqs. (2.32) through the product $E_\nu V(x)$, while for NSI with neutrons there is an extra dependence on $Y_n(x)$. Therefore, while the regions in the left panel in figure 1 span essentially a straight line, in the right panel the dependence is more complex.

In our past study [29], where only NSI with quarks were considered, neutrino evolution in the Sun was based on a fully numerical approach. In the present work, however, exploring the full parameter space of the most general NSI with protons, electrons, and neutrons

without assuming adiabaticity is challenging from the numerical point of view. To overcome this problem in our calculations we start by evaluating the adiabaticity index for the point in the NSI and oscillation parameter space to be surveyed. If for that point $\gamma^{-1}(x) < 1$ along the whole neutrino trajectory in the Sun we use the adiabatic approximation when computing the corresponding flavour transition probabilities and the subsequent prediction for all observables and χ^2 value. If, on the contrary, the adiabaticity condition is violated somewhere inside the Sun such point is removed from the parameter space to be surveyed. We do so because we have verified that for parameter values for which adiabaticity in the Sun is violated the predicted observables with the properly computed flavour transition probability without assuming adiabaticity never lead to good description of the data. But we also find that if one evaluates the probabilities for those parameters wrongly using the adiabatic approximation, one can find a “fake” good fit to the Solar and KamLAND data, which would lead to wrong conclusions about their acceptability. In conclusion, the adiabatic approximation can be safely used for the purposes of this work as long as one removes from the parameter space those points for which adiabaticity in the Sun is violated. Furthermore, once the data of atmospheric neutrino experiments is added to the fit, it totally disfavors the parameter regions where transitions in the Sun are not adiabatic.

2.2 Neutrino detection cross sections in the presence of NSI

In addition to propagation effects discussed above, non-standard interactions can also affect scattering in the detector. In this respect, it should be mentioned that all the atmospheric, reactor and accelerator experiments included in our fit rely on CC processes in order to detect neutrinos, so the corresponding cross-section is not affected by the NC-like NSI considered here.² This implies that the σ^{det} generalized cross-section matrix entering eq. (2.6) is diagonal in the SM flavour basis, and its non-zero entries coincide with the usual SM cross-section, that is,

$$\sigma^{\text{det}} = \text{diag}(\sigma_e^{\text{SM}}, \sigma_\mu^{\text{SM}}, \sigma_\tau^{\text{SM}}) \quad \text{for CC processes.} \quad (2.33)$$

Some solar neutrino experiments, on the contrary, are sensitive to NC NSI in some of the detection processes involved. This is the case of Borexino and SK (and SNO, albeit with lower sensitivity) which observe neutrino-electron ES, which may be affected by electron NSI. Regarding NSI with nuclei SNO can also probe axial-vector NSI in NC events, and CE ν NS experiments are able to set important constraints on vector interactions. In the rest of this section we review the phenomenological implications for these three cases separately.

2.2.1 Neutrino-electron elastic scattering

The presence of flavour-changing effects in NSI implies that the SM flavour basis no longer coincides with the interaction eigenstates of the neutrino-electron scattering. In such case

²It should be noted that a subleading component of NC interactions is present as background in many of these experiments, so that NSI parameter may in principle have an impact on the number of events. However, we expect these effects to be very small, so for simplicity we neglect them.

the generalized cross section σ^{det} can be obtained as the integral over the electron recoil kinetic energy T_e of the following matrix expression:

$$\frac{d\sigma^{\text{ES}}}{dT_e}(E_\nu, T_e) = \frac{2G_F^2 m_e}{\pi} \left\{ C_L^2 \left[1 + \frac{\alpha}{\pi} f_-(y) \right] + C_R^2 (1-y)^2 \left[1 + \frac{\alpha}{\pi} f_+(y) \right] - \{C_L, C_R\} \frac{m_e y}{2E_\nu} \left[1 + \frac{\alpha}{\pi} f_\pm(y) \right] \right\} \quad (2.34)$$

where $y \equiv T_e/E_\nu$ and f_+ , f_- , f_\pm are loop functions given in ref. [63], while α stands for the fine-structure constant and m_e is the electron mass. In this formula C_L and C_R are 3×3 hermitian matrices which incorporate both SM and NSI contributions:

$$C_{\alpha\beta}^L \equiv c_{L\beta} \delta_{\alpha\beta} + \varepsilon_{\alpha\beta}^{e,L} \quad \text{and} \quad C_{\alpha\beta}^R \equiv c_{R\beta} \delta_{\alpha\beta} + \varepsilon_{\alpha\beta}^{e,R}. \quad (2.35)$$

The effective couplings $c_{L\beta}$ and $c_{R\beta}$ account for the SM part, and contain both the flavour-universal NC terms and the ν_e -only CC scattering:

$$\begin{aligned} c_{Le} &= \rho \left[\kappa_e(T_e) \sin^2 \theta_w - \frac{1}{2} \right] + 1, & c_{Re} &= \rho \kappa_e(T_e) \sin^2 \theta_w, \\ c_{L\tau} &= c_{L\mu} = \rho \left[\kappa_\mu(T_e) \sin^2 \theta_w - \frac{1}{2} \right], & c_{R\tau} &= c_{R\mu} = \rho \kappa_\mu(T_e) \sin^2 \theta_w, \end{aligned} \quad (2.36)$$

with θ_w being the weak mixing angle, and ρ and $\kappa_\beta(T_e)$ departing from 1 due to radiative corrections of the gauge boson self-energies and vertices [63]. It is immediate to see that, if the NSI terms $\varepsilon_{\alpha\beta}^{e,L}$ and $\varepsilon_{\alpha\beta}^{e,R}$ are set to zero, the matrix $d\sigma^{\text{ES}}/dT_e$ becomes diagonal. Imposing the factorization of eq. (2.1) for the vector (+) and axial-vector (−) NSI we get:

$$\varepsilon_{\alpha\beta}^{e,V(A)} = \varepsilon_{\alpha\beta}^{e,L} \pm \varepsilon_{\alpha\beta}^{e,R} = \varepsilon_{\alpha\beta} \xi^e (\chi^L \pm \chi^R) = \sqrt{5} \cos \eta \sin \zeta (\chi^L \pm \chi^R) \varepsilon_{\alpha\beta}. \quad (2.37)$$

Let us finalize this section by discussing briefly the impact that the inclusion of NSI effects on ES could have on the generalized mass-ordering degeneracy discussed in section 2.1. We have seen that the parameter transformations (2.11) and (2.17) lead to a complex conjugation of the neutrino density matrix, $\rho^{\text{det}} \rightarrow [\rho^{\text{det}}]^*$. As shown in eq. (2.7), this does not affect the overall number of events (thus resulting in the appearance of the degeneracy) as long as it is accompanied by a similar transformation $\sigma^{\text{det}} \rightarrow [\sigma^{\text{det}}]^*$. The latter can be realized either as $C_L \rightarrow C_L^*$ and $C_R \rightarrow C_R^*$, which occur when both $\varepsilon_{\alpha\beta}^{e,L}$ and $\varepsilon_{\alpha\beta}^{e,R}$ undergo simple complex conjugation, or as $C_L \rightarrow -C_L^*$ and $C_R \rightarrow -C_R^*$, which require ad-hoc transformations of the diagonal entries $\varepsilon_{\alpha\alpha}^{e,L}$ and $\varepsilon_{\alpha\alpha}^{e,R}$ to compensate for the SM contribution of eq. (2.36). While conceptually identical to the situation occurring in neutrino oscillations, where the extra freedom introduced by NSI allows to “flip the sign” of the standard matter effects, the specific transformations required to achieve a perfect symmetry of σ^{det} differ from those of eq. (2.17). In principle one may first choose $\varepsilon_{\alpha\beta}^{e,L}$ and $\varepsilon_{\alpha\beta}^{e,R}$ accounting for eq. (2.36) and then tune $\varepsilon_{\alpha\beta}^{p,V}$ and $\varepsilon_{\alpha\beta}^{n,V}$ to fulfill eq. (2.17), but this procedure is incompatible with the factorization constraint of eq. (2.1), which assumes that all NSI have the same neutrino flavour structure independently of their chirality and of the charged fermion type. The net conclusion is that, for NSI involving electrons (that is, $\zeta \neq 0$) and assuming that the factorization in eq. (2.1) holds, ES effects *break* the generalized mass-ordering degeneracy.

2.2.2 SNO neutral-current cross-section

The SNO experiment observed NC interactions of solar neutrinos on deuterium. At low energies, the corresponding cross section is dominated by the Gamow-Teller transition and it scales as g_A^2 where g_A is the coupling of the neutrino current to the axial isovector hadronic current which in the SM is given by $g_A \equiv g_A^u - g_A^d$ [64–66]. Using that the nuclear corrections to g_A are the same when the NSI are added, we obtain that in the presence of the NC NSI we can write

$$\sigma^{\text{det}} = \sigma_{\text{SM}} \left(\frac{G_A}{g_A} \right)^2 \quad (2.38)$$

where G_A is an hermitian matrix in flavour space

$$\frac{G_A}{g_A} = \delta_{\alpha\beta} + \varepsilon_{\alpha\beta}^{u,A} - \varepsilon_{\alpha\beta}^{d,A} = \delta_{\alpha\beta} + \varepsilon_{\alpha\beta} (\xi^u - \xi^d) (\chi^L - \chi^R). \quad (2.39)$$

Clearly for vector NSI ($\chi^L = \chi^R$), the NSI contributions vanish and σ^{det} takes just the SM value times the identity in flavour space. Conversely for axial-vector NSI one gets $\chi^L - \chi^R = 1$ and the NSI term contributes.

2.2.3 Coherent elastic neutrino-nucleus scattering

The generalized cross-section σ^{det} describing CE ν NS in the presence of NSI can be obtained by integrating over the recoil energy of the nucleus E_R the following expression:

$$\frac{d\sigma^{\text{coh}}(E_R, E_\nu)}{dE_R} = \frac{G_F^2}{2\pi} Q^2 F^2(q^2) m_A \left(2 - \frac{m_A E_R}{E_\nu^2} \right) \quad (2.40)$$

where m_A is the mass of the nucleus and $F(q^2)$ is its nuclear form factor evaluated at the squared momentum transfer of the process, $q^2 = 2m_A E_R$. In this formalism, the structure in flavour space which characterizes σ^{det} is encoded into the hermitian matrix \mathcal{Q} , which is just the generalization of the weak charge of the nucleus for this formalism. For a nucleus with Z protons and N neutrons, it reads:

$$\mathcal{Q}_{\alpha\beta} = Z(g_p^V \delta_{\alpha\beta} + \varepsilon_{\alpha\beta}^{p,V}) + N(g_n^V \delta_{\alpha\beta} + \varepsilon_{\alpha\beta}^{n,V}) \quad (2.41)$$

where $g_p^V = 1/2 - 2\sin^2\theta_w$ and $g_n^V = -1/2$ are the SM vector couplings to protons and neutrons, respectively. In experiments with very short baselines such as those performed so far, neutrinos have no time to oscillate and therefore the density matrix at the detector ρ^{det} is just the identity matrix. Taking this explicitly into account in eq. (2.6) we get:

$$\rho^{\text{det}} = I \quad \Rightarrow \quad N_{\text{ev}} \propto \mathcal{Q}_\alpha^2 \quad \text{with} \quad \mathcal{Q}_\alpha^2 \equiv [\mathcal{Q}^2]_{\alpha\alpha} = (\mathcal{Q}_{\alpha\alpha})^2 + \sum_{\beta \neq \alpha} |\mathcal{Q}_{\alpha\beta}|^2 \quad (2.42)$$

for incident neutrino flavour α , thus recovering the expressions for the ordinary weak charges \mathcal{Q}_α^2 used in our former publications. Coming back to eq. (2.41), let us notice that it can be rewritten as:

$$\mathcal{Q}_{\alpha\beta} = Z[(g_p^V + Y_n^{\text{coh}} g_n^V) \delta_{\alpha\beta} + \varepsilon_{\alpha\beta}^{\text{coh}}] \quad \text{with} \quad \varepsilon_{\alpha\beta}^{\text{coh}} \equiv \varepsilon_{\alpha\beta}^{p,V} + Y_n^{\text{coh}} \varepsilon_{\alpha\beta}^{n,V} \quad (2.43)$$

where $Y_n^{\text{coh}} \equiv N/Z$ is the neutron/proton ratio characterizing the target of a given CE ν NS experiment. Imposing the quark-lepton factorization of eq. (2.1) we get:

$$\varepsilon_{\alpha\beta}^{\text{coh}} = \varepsilon_{\alpha\beta}(\xi^p + Y_n^{\text{coh}}\xi^n)(\chi^L + \chi^R) = \sqrt{5} [\cos \eta \cos \zeta + Y_n^{\text{coh}} \sin \eta] (\chi^L + \chi^R) \varepsilon_{\alpha\beta}. \quad (2.44)$$

Similarly to eq. (2.19), this expression suggests that the analysis of coherent scattering data can be performed in terms of the effective couplings $\varepsilon_{\alpha\beta}^{\text{coh}}$, whose best-fit value and allowed ranges are independent of (η, ζ) . As a consequence, the bounds on $\varepsilon_{\alpha\beta}$ simply scale as $[\cos \eta \cos \zeta + Y_n^{\text{coh}} \sin \eta]$. In analogy to eq. (2.16), one can define an effective angle $\tan \eta'' \equiv \tan \eta / \cos \zeta$ parametrizing the direction in the (ξ^p, ξ^n) plane, such that all CE ν NS experiments depend on (η, ζ) only through the combination η'' . In particular, it is straightforward to see that a coherent scattering experiment characterized by a given Y_n^{coh} ratio will yield no bound on $\varepsilon_{\alpha\beta}$ for $\eta'' = \arctan(-1/Y_n^{\text{coh}})$, as for this value the effects of NSI on protons and neutrons cancel exactly. Such a cancellation can be obtained, for example, for models of the type proposed in ref. [21], where the Z' associated to a new gauge symmetry also has a sizable kinetic mixing with the SM photon, which allows for arbitrary relative size of NSI with up and down quarks.

3 Results

This section summarizes the main results of our study. In section 3.1 we first review the data included in the fit, introduce our χ^2 definition, and outline the details related to the sampling of the multi-dimensional parameter space. We then proceed to present our results for NSI with electrons (section 3.2), with quarks (section 3.3), and for simultaneous NSI with electrons and quarks (section 3.4). The status of the LMA-D solution in this general case is discussed in section 3.5.

3.1 Simulation details

The data samples included in our oscillation analysis mostly coincide with those in NuFIT-5.2 [67]. In brief, in the analysis of solar neutrino data we consider the total rates from the radiochemical experiments Chlorine [68], Gallex/GNO [69], and SAGE [70], the spectral data (including day-night information) from the four phases of Super-Kamkoikande in refs. [71–74], the results of the three phases of SNO in the form of the day-night spectrum data of SNO-I [75], and SNO-II [76] and the three total rates of SNO-III [77],³ and the spectra from Borexino Phase-I [79, 80], and Phase-II [81]. For reactor neutrinos we include the separate DS1, DS2, DS3 spectra from KamLAND [82] with Daya Bay reactor

³This corresponds to the analysis labeled SNO-DATA in ref. [28]. In that article an alternative analysis of the SNO data was introduced, labeled SNO-POLY, based on an effective *MSW-like* polynomial parametrization for the day and night survival probabilities of the combined SNO phases I–III, as detailed in ref. [78]. The SNO-POLY approach can be efficiently used as long as NSI only enter in propagation through the matter potential, and therefore in the subsequent analysis [29, 47] the SNO results were included in this way. However, the polynomial parametrization of SNO-POLY cannot account for NSI effects in neutrino interactions, so that in the present work we have reverted to the full SNO-DATA version of the SNO analysis. This leads to small differences in the results of the analysis with couplings to quarks only with respect to those in refs. [29, 47].

ν fluxes [83], the FD/ND spectral ratio, with 1276-day (FD), 587-day (ND) exposures of Double-Chooz [84], the 3158-day separate EH1, EH2, EH3 spectra [85] of Daya-Bay, and the 2908-day FD/ND spectral ratio of RENO [86]. For atmospheric neutrinos we use the four phases of Super-Kamiokande (up to 1775 days of SK4 [87]), the complete set of DeepCore 3-year μ -like events presented in ref. [88] and publicly released in ref. [89], and the results on ν_μ -induced upgoing muons reported by IceCube [90] based on one year of data taking. Finally, for LBL experiments we include the final neutrino and antineutrino spectral data on ν_e -appearance and ν_μ -disappearance in MINOS [91], the 19.7×10^{20} pot ν_μ -disappearance and 16.3×10^{20} pot $\bar{\nu}_\mu$ -disappearance data in T2K [92], and the 13.6×10^{20} pot ν_μ -disappearance and 12.5×10^{20} pot $\bar{\nu}_\mu$ -disappearance data in NO ν A [93]. Notice that to ensure full consistency with our CP-conserving parametrization we have chosen not to include in the present study the data from the ν_e and $\bar{\nu}_e$ appearance channels in NO ν A and T2K. With this data we construct $\chi^2_{\text{OSC}}(\vec{\omega}, \vec{\epsilon})$ where we denote by $\vec{\omega}$ the 3ν oscillation parameters and $\vec{\epsilon}$ the NSI parameters considered in the analysis.

When combining with CE ν NS we include the results from COHERENT data on CsI [46, 48] and Ar targets [49, 55] (see refs. [47, 52] for details). In particular, for the analysis of COHERENT CsI data we use the quenching factor from ref. [94] and the nuclear form factor from ref. [95]. For the analysis of COHERENT Ar data we use the quenching factor provided by the COHERENT collaboration in ref. [55] and Helm [96] nuclear form factor (the values of the parameters employed are the same as in ref. [52]). For CE ν NS searches using reactor neutrinos at Dresden-II reactor experiment [56] we follow the analysis presented in ref. [52] with YBe quenching factor [97] (the characteristic momentum-transfer in this experiment is very low so the nuclear form factor can be taken to be 1). With all this we construct the corresponding $\chi^2_{\text{COH,CsI}}(\vec{\epsilon})$, $\chi^2_{\text{COH,Ar}}(\vec{\epsilon})$, and $\chi^2_{\text{D-II,Ge}}(\vec{\epsilon})$.

Our goal is to find the global minimum of the total χ^2 which, unless otherwise stated, is obtained adding the contributions from our global analysis of oscillation data («GLOB-OSC w NSI in ES») and CE ν NS data:

$$\chi^2(\vec{\omega}, \vec{\epsilon}) = \chi^2_{\text{OSC}}(\vec{\omega}, \vec{\epsilon}) + \chi^2_{\text{CE}\nu\text{NS}}(\vec{\epsilon}) \tag{3.1}$$

where we have defined

$$\chi^2_{\text{CE}\nu\text{NS}} = \chi^2_{\text{COH,CsI}} + \chi^2_{\text{COH,Ar}} + \chi^2_{\text{D-II,Ge}}. \tag{3.2}$$

The minimum of the total χ^2 is obtained after minimization over all the nuisance parameters, which are included as pull terms in our fit.⁴ However, note that a priori it is possible to suppress the effects of vector NSI in neutrino detection while still allowing for sizable NSI in oscillations, since the momentum transfer required for the effects to be observable is not the same in the two cases [15]. The paradigmatic example of BSM scenarios leading to sizable NSI are models with light mediators. Matter effects arise from a coherent effect, that is, with zero momentum-transfer, and therefore apply to NSI induced by ultra light mediators, as long as their mass is $M_{\text{med}} \gtrsim 1/R_\oplus \sim \mathcal{O}(10^{-12})$ eV [25, 98]. Scattering effects, on the contrary, require a minimum momentum-transfer to be observable:

⁴For details on the numerical implementation of systematic uncertainties see refs. [52, 54, 67].

- In the case of ES, for recoil energies $T_e \simeq \mathcal{O}(500 \text{ keV})$ (which are in the right ballpark for Borexino) the relevant scale is $q = \sqrt{2m_e T_e} \sim \mathcal{O}(500 \text{ keV})$. Therefore, in what follows we will also present our results neglecting the effects due to NSI in detection («GLOB-OSC w/o NSI in ES»), so as to consider this class of models with very light mediators, $M_{\text{med}} \ll \mathcal{O}(500 \text{ keV})$. For SNO and SK, sensitive to neutrinos with higher energies, a similar argument leads to $q \sim \mathcal{O}(5\text{--}10 \text{ MeV})$. Hence, results labeled as «GLOB-OSC w NSI in ES» apply to NSI generated by models with $M_{\text{med}} \gtrsim 10 \text{ MeV}$, where we expect to have NSI effects on the detection through ES for all solar experiments considered in this work. Finally, in the intermediate mass range only Borexino would be fully sensitive to NSI effects on detection.
- In the case of CE ν NS, the relevant momentum transfer also depends on the experiment considered. For COHERENT data on CsI (Ar), this can be estimated as $q \sim 50 \text{ MeV}$ ($q \sim 30 \text{ MeV}$) while for Dresden-II we get $q \sim \mathcal{O}(5 \text{ MeV})$. Therefore, in section 3.3 we will present our results using the combination of all oscillation and CE ν NS data, sensitive to models with $M_{\text{med}} \gtrsim 50 \text{ MeV}$ («GLOB-OSC+CE ν NS»), as well as the results for oscillation data alone, sensitive to NSI models with $M_{\text{med}} \ll 5 \text{ MeV}$ (labeled as «GLOB-OSC»). In the intermediate mass range between 5 and 50 MeV, effects on CE ν NS may be suppressed for some experiments but not all of them.

The intermediate mass ranges defined above (where NSI effects in detection may be observed at one experiment, but not another) require special handling and are therefore beyond the scope of the present paper, leaving them for future work.

In the axial-vector case there are no NSI effects in oscillations nor CE ν NS and the NSI parameters only enter in the ES and/or NC detection cross sections. Thus for axial-vector NSI with electrons the derived bounds apply for mediator masses as discussed above for ES. NC interactions in SNO occur for neutrinos with energy above the binding energy of the deuteron, 2.22 MeV. So the bounds for axial-vector NSI with quarks derived here apply for $M_{\text{med}} \gtrsim 3 \text{ MeV}$.

Let us finalize this discussion by briefly reviewing the number of parameters involved in the fit. A priori, under the approximations assumed in the present work, atmospheric and long-baseline experiments depend on all the oscillation parameters as well as on the NSI variables defined in eqs. (2.21). However, for LBL experiments we fix Δm_{21}^2 and $|\theta_{12} - 45^\circ|$ to their SM best-fit value, as their relevance for such data is only subleading and we know from previous studies [29] that NSI are not going to spoil their determination sizably (except for the θ_{12} octant which we do *not* fix, hence the absolute value in the corresponding fixed value above). For the analysis of atmospheric neutrinos we further set $\Delta m_{21}^2 \rightarrow 0$, so the dependence on θ_{12} and δ_{CP} vanishes. With this, neutrino propagation through the Earth is described in terms of six continuous parameters, namely $(\Delta m_{31}^2, \theta_{13}, \theta_{23})$ for the vacuum part and $(\varepsilon_{\oplus}, \varphi_{12}, \varphi_{13})$ for the matter part, as well as the two CP-conserving values of δ_{CP} and the two options for the θ_{12} octant. We additionally fix the value of θ_{13} to the present best fit, as its determination comes mainly from reactor experiments for which NSI effects are suppressed. On the other hand, neutrino oscillations in solar and KamLAND data depend effectively on ε_D and ε_N for the matter part, while the vacuum part depends

on θ_{12} , θ_{23} , Δm_{21}^2 and the two-CP conserving values of δ_{CP} (θ_{13} is also fixed to its best-fit value here). Finally note that, while oscillations depend on differences between the diagonal NSI parameters, the addition of scattering effects in detection breaks this pattern. This implies that in addition to the two differences in eqs. (2.19) we need to scan one of the diagonal parameters, which we take to be $\varepsilon_{\mu\mu}^{\oplus}$. The last two parameters of relevance are the two angles η and ζ , which determine the direction of NSI in (ξ^e, ξ^p, ξ^n) space.

Taking into account all of the above, in our simulations we scan the multi-dimensional space spanned by the following continuous parameters:

$$\theta_{12}, \theta_{23}, \Delta m_{21}^2, \Delta m_{31}^2, \varepsilon_{\oplus}, \varphi_{12}, \varphi_{23}, \varepsilon_{\mu\mu}^{\oplus}, \eta, \zeta, \tag{3.3}$$

as well as the two CP-conserving values of $\delta_{\text{CP}} \in \{0, \pi\}$. In order to scan this multi-dimensional parameter space efficiently, we make use of the MultiNest [99, 100] and Diver [101] algorithms.

3.2 New constraints on NSI with electrons

We start by describing the results of the global analysis for the case of NSI with electrons, which, as mentioned in the introduction, was not considered in our previous studies [28, 29, 47]. We plot in figure 2 and 3 the constraints on the different coefficients for the two scenarios outlined in the previous section, without and with NSI effects in the detection cross section, respectively.⁵ The corresponding 90% CL allowed ranges are listed in table 1 and on the left columns in table 2 respectively.

The first thing to notice is that in the scenario «GLOB-OSC w/o NSI in ES», for the flavour diagonal coefficients, only the combinations $\varepsilon_{ee}^{e,V} - \varepsilon_{\mu\mu}^{e,V}$ and $\varepsilon_{\tau\tau}^{e,V} - \varepsilon_{\mu\mu}^{e,V}$ can be constrained, and two separate allowed ranges appear (see bottom row in figure 2): one around $\varepsilon_{ee}^{e,V} - \varepsilon_{\mu\mu}^{e,V} \sim 0$ and another around $\varepsilon_{ee}^{e,V} - \varepsilon_{\mu\mu}^{e,V} \sim -2$. This is nothing else than the result of the generalized mass-ordering degeneracy of eq. (2.17). The two disjoint allowed solutions correspond to regions of oscillation parameters with $\theta_{12} < 45^\circ$ (with ranges labeled «LMA» in table 1) and with $\theta_{12} > 45^\circ$ (with ranges labeled «LMA-D» in table 1) respectively. As discussed in section 2.1, the degeneracy is partly broken by the variation of chemical composition of the matter along the neutrino trajectory when NSI coupling to neutrons are involved. But in this case, with only coupling to electrons, the degeneracy is perfect as can be seen by the fact that $\Delta\chi^2 = 0$ in both minima of $\varepsilon_{ee}^{e,V} - \varepsilon_{\mu\mu}^{e,V}$. From the panels on the lower row we observe that the projection of the allowed regions corresponding to each of the two solutions partly overlap for $\varepsilon_{\tau\tau}^{e,V} - \varepsilon_{\mu\mu}^{e,V}$ and $\varepsilon_{\alpha\neq\beta}^{e,V}$, which leads to the non-trivial shapes of some of the corresponding two-dimensional regions for some pairs of those parameters.

The results for the scenario «GLOB-OSC w NSI in ES» in figure 2, and on the left columns in table 2, show that the inclusion of the effect of the vector NSI in the ES cross sections in Borexino, SNO, and SK totally lifts the degeneracy. In this scenario only the LMA solution is allowed, and $\varepsilon_{ee}^{e,V}$, $\varepsilon_{\mu\mu}^{e,V}$, and $\varepsilon_{\tau\tau}^{e,V}$ can be independently constrained. Notice also that in this case, the lifting of the LMA-D solution leads to allowed regions with more

⁵Notice that from the point of view of the data analysis the results from the «GLOB-OSC w/o NSI in ES» are totally equivalent to those obtained for vector NSI which couple only to protons.

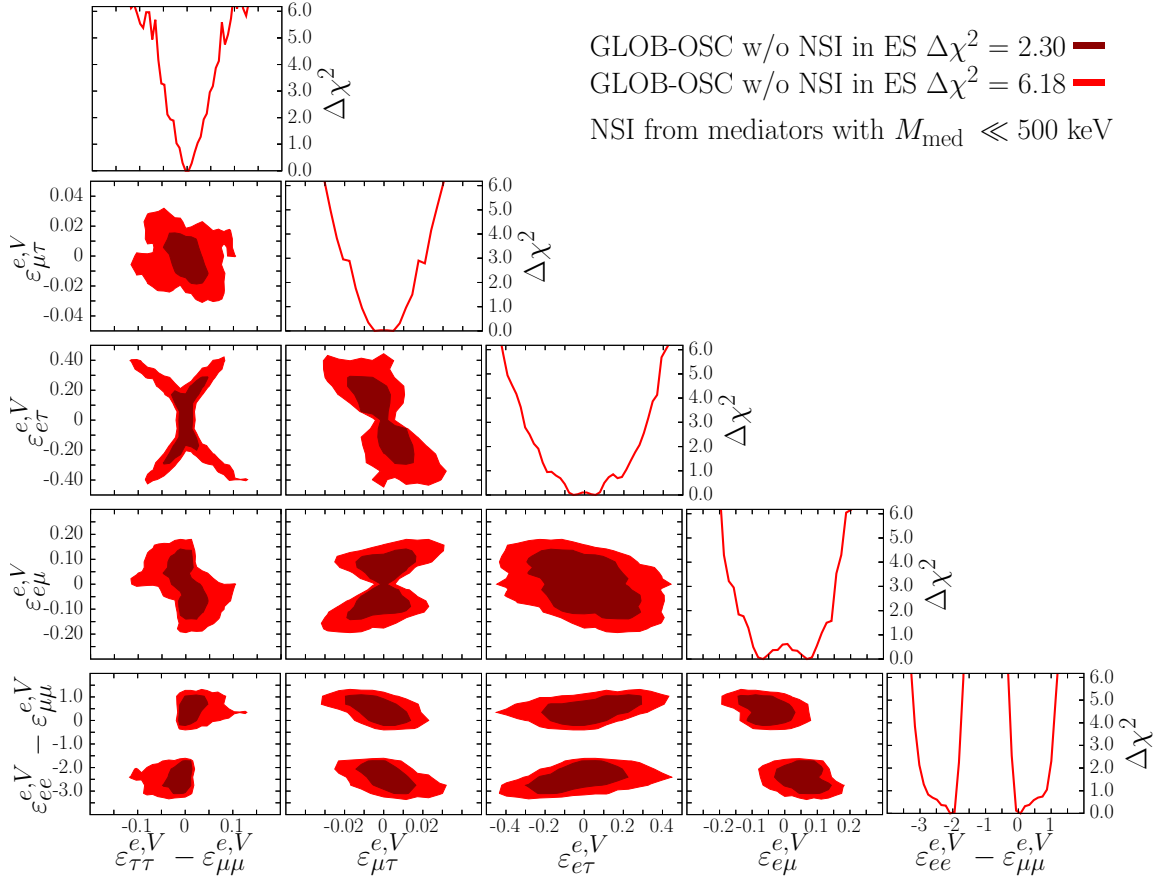


Figure 2. Constraints on the coefficients for vector NSI with electrons from the global analysis of oscillation data *without including the effect of NSI in the detection cross section*. Each panel shows a two-dimensional projection of the allowed multi-dimensional parameter space after minimization with respect to the undisplayed parameters. The regions correspond to 1σ and 2σ (2 d.o.f.).

	Allowed ranges at 90% CL (marginalized)	
	GLOB-OSC w/o NSI in ES	
	LMA	LMA \oplus LMA-D
$\varepsilon_{ee}^{e,V} - \varepsilon_{\mu\mu}^{e,V}$	$[-0.21, +1.0]$	$[-3.0, -1.8] \oplus [-0.21, +1.0]$
$\varepsilon_{\tau\tau}^{e,V} - \varepsilon_{\mu\mu}^{e,V}$	$[-0.015, +0.048]$	$[-0.040, +0.047]$
$\varepsilon_{e\mu}^{e,V}$	$[-0.15, +0.035]$	$[-0.15, +0.14]$
$\varepsilon_{e\tau}^{e,V}$	$[-0.21, +0.31]$	$[-0.29, +0.31]$
$\varepsilon_{\mu\tau}^{e,V}$	$[-0.020, +0.012]$	$[-0.020, +0.017]$

Table 1. 90% CL bounds (1 d.o.f., 2-sided) on the coefficients of NSI operators with electrons after marginalizing over all other NSI and oscillation parameters. The bounds are derived from the global analysis of oscillation data *without including the effect of NSI in the ES cross section* (NSI induced by mediators with mass $M_{\text{med}} \ll 500$ keV, see section 3.1). The ranges in the first column (labeled «LMA») correspond to an analysis in which we restrict $\theta_{12} < 45^\circ$. In the second column (labeled «LMA \oplus LMA-D»), both $\theta_{12} < 45^\circ$ and $\theta_{12} > 45^\circ$ are allowed. The same bounds hold for vector NSI with protons.

	Allowed ranges at 90% CL (marginalized)			
	Vector ($X = V$)		Axial-vector ($X = A$)	
	Borexino	GLOB-OSC w NSI in ES	Borexino	GLOB-OSC w NSI in ES
$\varepsilon_{ee}^{e,X}$	$[-1.1, +0.17]$	$[-0.13, +0.10]$	$[-0.38, +0.24]$	$[-0.13, +0.11]$
$\varepsilon_{\mu\mu}^{e,X}$	$[-2.4, +1.5]$	$[-0.20, +0.10]$	$[-1.5, +2.4]$	$[-0.70, +1.2]$
$\varepsilon_{\tau\tau}^{e,X}$	$[-2.8, +2.1]$	$[-0.17, +0.093]$	$[-1.8, +2.8]$	$[-0.53, +1.0]$
$\varepsilon_{e\mu}^{e,X}$	$[-0.83, +0.84]$	$[-0.097, +0.011]$	$[-0.79, +0.76]$	$[-0.41, +0.40]$
$\varepsilon_{e\tau}^{e,X}$	$[-0.90, +0.85]$	$[-0.18, +0.080]$	$[-0.81, +0.78]$	$[-0.36, +0.36]$
$\varepsilon_{\mu\tau}^{e,X}$	$[-2.1, +2.1]$	$[-0.0063, +0.016]$	$[-1.9, +1.9]$	$[-0.79, +0.81]$

Table 2. 90% CL bounds (1 d.o.f., 2-sided) on the coefficients of vector NSI operators with electrons after marginalizing over all other NSI and oscillation parameters. The bounds are derived from the global analysis of oscillation data *including the effect of NSI in the ES cross section*. For comparison, the results obtained from the analysis of Borexino Phase-II data in ref. [54] are also shown for comparison. Note that these bounds apply to interactions induced by mediators with masses $M_{\text{med}} \gtrsim 10$ MeV, see section 3.1.

standard (close-to-elliptical) shapes. For the sake of comparison we show for this scenario the corresponding bounds derived from the analysis of Borexino spectra in ref. [54]. The comparison shows that for vector NSI with electrons the global analysis of the oscillation data reduces the allowed ranges of the NSI coefficients by factors ~ 4 –200 with respect to those derived with Borexino spectrum only. In other words, the NSI contribution to ES is important to break the LMA-D degeneracy and to impose independent bounds on the three flavour-diagonal NSI coefficients, but within the LMA solution the effect of the vector NSI on the matter potential also leads to stronger constraints. This is further illustrated by the results obtained for the analysis with axial-vector NSI which are shown in figure 4 and right columns in table 2. Axial-vector NSI do not contribute to the matter potential and therefore the difference between the results of the global oscillation and the Borexino-only analysis in this case arises solely from the effect of the axial-vector NSI on the ES cross section in SNO and SK. Comparing the red and green regions in figure 4 and the two left columns in table 2 we see that for axial-vector NSI the improvement over the bounds derived with Borexino-only analysis is just a factor ~ 2 –3.

3.3 Updated constraints on NSI with quarks

Next we briefly summarize the results of the analysis for the scenarios of NSI with either up or down quarks (more general combinations of couplings to quarks and electrons will be presented in the next section). For vector NSI this updates and complements the results presented in refs. [29, 47] by accounting for the effects of increased statistics in the oscillation experiments, including the addition of new data from Borexino Phase-II. Notice also that in the present analysis, as mentioned above, the treatment of the SNO data is different than in refs. [29, 47]. Furthermore when combining with CE ν NS we include here the results from

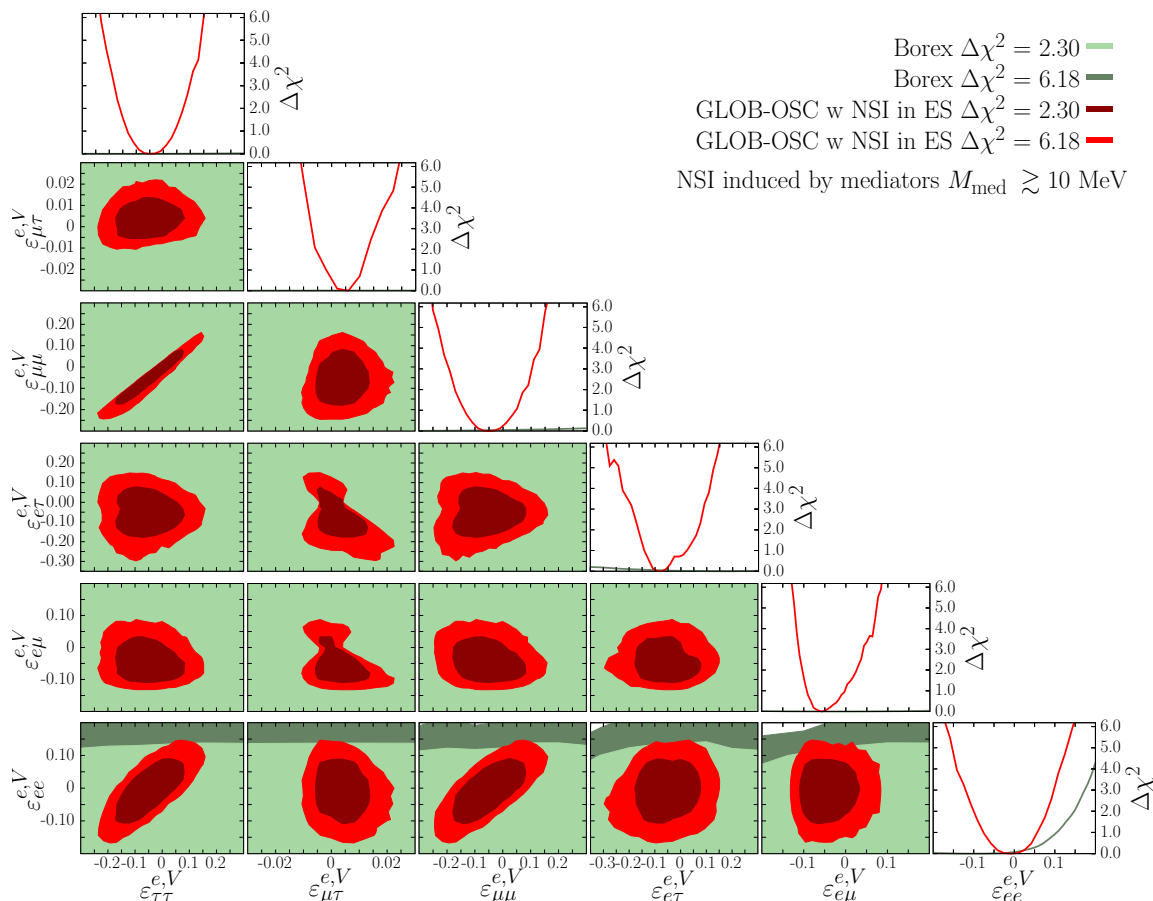


Figure 3. Constraints on the coefficients for vector NSI with electrons from the global analysis of oscillation data *including the effect of NSI in the ES cross section*. Each panel shows a two-dimensional projection of the allowed multi-dimensional parameter space after minimization with respect to the undisplayed parameters. The contours correspond to 1σ and 2σ (2 d.o.f.). The closed red regions correspond to the global oscillation analysis which involves the six NSI plus five oscillation parameters. For the sake of comparison we also show as green regions the constraints obtained from the analysis of full Borexino Phase-II spectrum in ref. [54].

COHERENT both on CsI [46, 48] and Ar targets [49, 55], together with the recent results from CE ν NS searches using reactor neutrinos at Dresden-II reactor experiment [52, 56].

Let us start discussing the complementary sensitivity to vector-NSI from the combined CE ν NS results with that from present oscillation data, for general models leading to NSI with quarks. With this aim we have first performed an analysis including only the effect of vector NSI on the matter potential in the neutrino oscillation experiments. The results of such analysis are given in the left column of table 5 in terms of the allowed ranges of the effective NSI couplings to the Earth matter, $\varepsilon_{\alpha\beta}^{\oplus}$, defined in eq. (2.18) (see section 3.4 for details). Comparison with the constraints from all available CE ν NS data is illustrated in figure 5 where we plot the allowed regions in the plane $(\varepsilon_{ee}^{\oplus}, \varepsilon_{\mu\mu}^{\oplus})$. The figure shows the allowed regions obtained by the analysis of each of the two sets of data *independently*, after

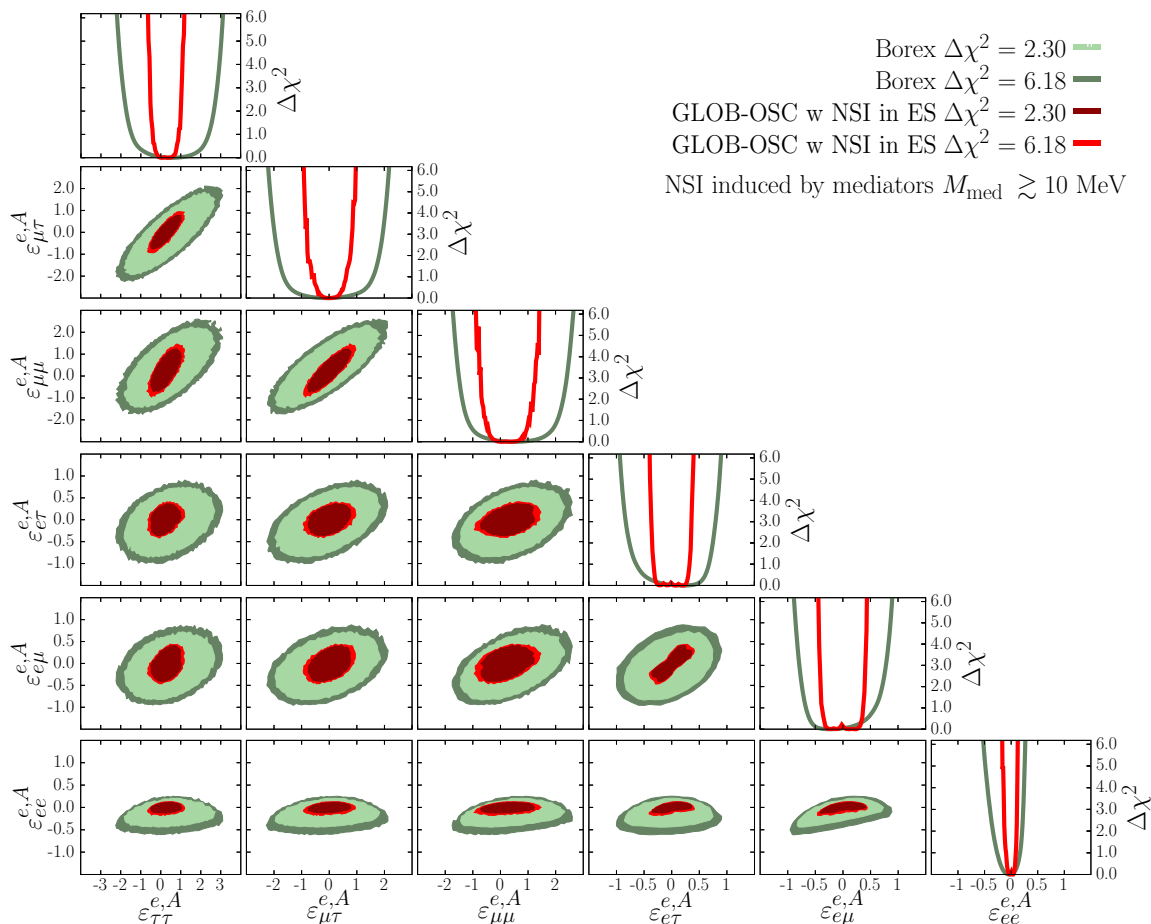


Figure 4. Same as figure 3 but for Axial-vector NSI.

marginalization over the all other (including off-diagonal) NSI parameters.⁶ As discussed in section 2.2.3, even when considering NSI coupling only to quarks, there is always a value of η for which the contribution of NSI to the CE ν NS cross section cancels. Consequently CE ν NS data with a single nucleus does not lead to any constraint on the $\varepsilon_{\alpha\beta}^{\oplus}$ parameters. However, the cancellation occurs at different values of η for the three nucleus considered (CsI, Ar, and Ge), and consequently, as seen in the figure, the combination of CE ν NS data with the three nuclear targets does constrain the full space of effective $\varepsilon_{\alpha\beta}^{\oplus}$, even after marginalization over η . The constraints derived from the combined CE ν NS data are independent (and complementary) to those provided by the oscillation analysis and, as seen in the figure, they are fully consistent.

The allowed ranges for vector NSI with up or down quarks are compiled in table 3 and show good qualitative agreement with those of refs. [29, 47], with the expected small deviations due to the differences in the analysis, quoted CL, and included data.

⁶Technically the regions for oscillations in figure 5 are obtained by performing each of the two analysis in terms of the 9 (out of the 10) basic parameters listed in eq. (3.3) (fixing $\zeta = 0$) including the corresponding value of Y_n to each data sample. Therefore the output of each analysis is a χ^2 function of the basic 9 parameters, which is then marginalized with respect to all parameters except for the two combinations shown in the figure.

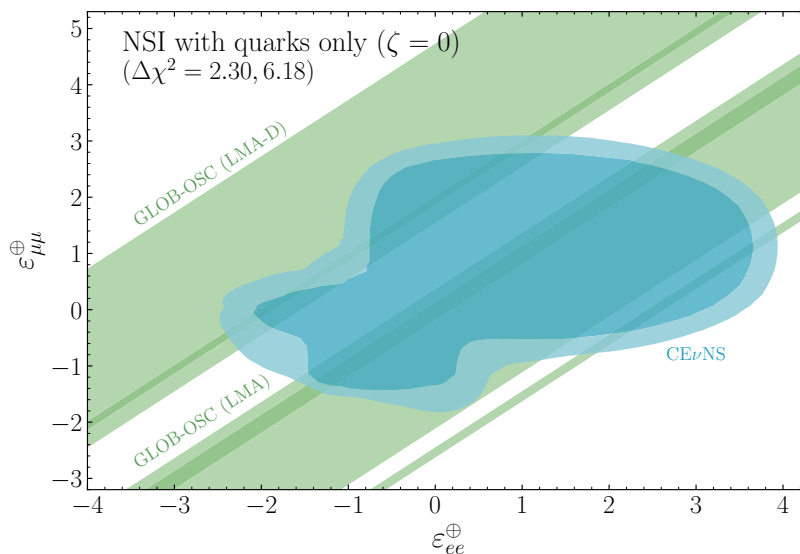


Figure 5. Allowed regions in the plane of $\varepsilon_{ee}^{\oplus}$ and $\varepsilon_{\mu\mu}^{\oplus}$ for vector NSI with quarks from the combinations of CE ν NS data compared with the allowed regions from the global oscillation analysis which are the two diagonal shaded bands corresponding to the LMA and LMA-D solutions. Both the green and blue regions are obtained after *independently* marginalizing over all other relevant parameters: NSI couplings (including η) for the CE ν NS region, and NSI couplings, η and oscillation parameters for the «GLOB-OSC» regions. So the values of other NSI and η in the blue and green regions are not forced to be the same.

Finally for completeness we have also performed a new dedicated analysis including axial-vector NSI with up or down quarks. Axial-vector NSI with quarks do not contribute to matter effects nor to CE ν NS. They only enter the global analysis via their modification of the NC event rate in the SNO experiment (see section 2.2.2), which is not able to constrain the NSI coefficients if all of them are included simultaneously due to possible cancellations between their respective contributions to the NC rate. Thus in this case we derive the bounds *assuming that only one NSI coupling is different from zero at a time*. The corresponding allowed ranges can be found in table 4.

As seen in the table, for all the coefficients, the allowed range is composed of several disjoint intervals. They correspond to values of the NSI couplings for which the SNO-NC event rate is approximately the SM prediction. This can occur for either flavour diagonal or flavour non-diagonal coefficients because solar neutrinos reach the Earth as mass eigenstates, so the density matrix describing the neutrino state at the detector is diagonal in the mass basis, but not in the flavor basis. The presence of non-vanishing off-diagonal $\rho_{\alpha\neq\beta}$ elements is responsible for the sensitivity to off-diagonal $\varepsilon_{\alpha\neq\beta}$ coefficients. More quantitatively, the ranges correspond to coefficients verifying:

$$0 \simeq \text{Tr} \left[\rho^{\text{SNO}} \left(\frac{G_A}{g_A} \right)^2 \right] - 1 = \begin{cases} \rho_{\alpha\alpha}^{\text{SNO}} [(\varepsilon_{\alpha\alpha}^{q,A})^2 \pm 2\varepsilon_{\alpha\alpha}^{q,A}], \\ (\rho_{\alpha\alpha}^{\text{SNO}} + \rho_{\beta\beta}^{\text{SNO}}) (\varepsilon_{\alpha\neq\beta}^{q,A})^2 \pm 4 \text{Re}(\rho_{\alpha\neq\beta}^{\text{SNO}}) \varepsilon_{\alpha\neq\beta}^{q,A} \end{cases} \quad (3.4)$$

where the upper line holds when the NSI coefficient included is flavour diagonal, and the lower one when it is flavour-changing and the \pm sign correspond to $q = u$ and $q = d$

	Allowed ranges at 90% CL (marginalized)		Allowed ranges at 90% CL (marginalized)
	GLOB-OSC		
	LMA	LMA \oplus LMA-D	LMA = LMA \oplus LMA-D
$\epsilon_{ee}^{u,V} - \epsilon_{\mu\mu}^{u,V}$	$[-0.063, +0.36]$	$[-1.1, -0.79] \oplus [-0.063, +0.36]$	$[-0.038, +0.034] \oplus [+0.34, +0.42]$
$\epsilon_{\tau\tau}^{u,V} - \epsilon_{\mu\mu}^{u,V}$	$[-0.0053, +0.017]$	$[-0.021, +0.018]$	$[-0.046, +0.031] \oplus [+0.35, +0.42]$
$\epsilon_{e\mu}^{u,V}$	$[-0.057, +0.013]$	$[-0.057, +0.061]$	$[-0.046, +0.033] \oplus [+0.35, +0.42]$
$\epsilon_{e\tau}^{u,V}$	$[-0.076, +0.11]$	$[-0.12, +0.11]$	$[-0.044, +0.0049]$
$\epsilon_{\mu\tau}^{u,V}$	$[-0.0077, +0.0042]$	$[-0.0077, +0.0083]$	$[-0.079, +0.11]$
$\epsilon_{ee}^{d,V} - \epsilon_{\mu\mu}^{d,V}$	$[-0.069, +0.38]$	$[-1.3, -0.91] \oplus [-0.072, +0.38]$	$[-0.036, +0.031] \oplus [+0.30, +0.39]$
$\epsilon_{\tau\tau}^{d,V} - \epsilon_{\mu\mu}^{d,V}$	$[-0.0058, +0.018]$	$[-0.029, +0.019]$	$[-0.040, +0.038] \oplus [+0.31, +0.39]$
$\epsilon_{e\mu}^{d,V}$	$[-0.058, +0.014]$	$[-0.058, +0.098]$	$[-0.041, +0.043] \oplus [+0.31, +0.39]$
$\epsilon_{e\tau}^{d,V}$	$[-0.079, +0.11]$	$[-0.16, +0.11]$	$[-0.054, +0.0045]$
$\epsilon_{\mu\tau}^{d,V}$	$[-0.0087, +0.0051]$	$[-0.0087, +0.015]$	$[-0.051, +0.11]$
			$[-0.0075, +0.0046]$

Table 3. 90% allowed ranges for the vector NSI couplings $\epsilon_{\alpha\beta}^{u,V}$ and $\epsilon_{\alpha\beta}^{d,V}$ as obtained from the global analysis of oscillation data (left columns, applicable to NSI induced by mediators with $M_{\text{med}} \ll 5$ MeV) and also including data from CE ν NS experiments (right columns, applicable to NSI induced by mediators with $M_{\text{med}} \gtrsim 50$ MeV). The results are obtained after marginalizing over oscillation and the other matter potential parameters either within the LMA only ($\theta_{12} < 45^\circ$) and within both LMA ($\theta_{12} < 45^\circ$) and LMA-D ($\theta_{12} > 45^\circ$) subspaces respectively (this second case is denoted as LMA \oplus LMA-D). Notice that once CE ν NS data is included the two columns become identical, since for NSI couplings with $f = u, d$ the LMA-D solution is only allowed well above 90% CL.

Allowed ranges at 90% CL (1-parameter)		
GLOB-OSC		
$\varepsilon_{ee}^{u,A}$	$[-2.1, -1.8] \oplus [-0.19, +0.13]$	$-\varepsilon_{ee}^{d,A}$
$\varepsilon_{\mu\mu}^{u,A}$	$[-2.2, -1.7] \oplus [-0.26, +0.18]$	$-\varepsilon_{\mu\mu}^{d,A}$
$\varepsilon_{\tau\tau}^{u,A}$	$[-2.1, -1.8] \oplus [-0.20, +0.15]$	$-\varepsilon_{\tau\tau}^{d,A}$
$\varepsilon_{e\mu}^{u,A}$	$[-1.5, -1.2] \oplus [-0.16, +0.12] \oplus [+1.4, +1.7]$	$-\varepsilon_{e\mu}^{d,A}$
$\varepsilon_{e\tau}^{u,A}$	$[-1.5, -1.3] \oplus [-0.13, +0.10] \oplus [+1.4, +1.7]$	$-\varepsilon_{e\tau}^{d,A}$
$\varepsilon_{\mu\tau}^{u,A}$	$[-0.085, +0.11] \oplus [+1.6, +1.9]$	$-\varepsilon_{\mu\tau}^{d,A}$

Table 4. 90% CL bounds (1 d.o.f., 2-sided) on the effective axial-vector NSI couplings with quarks. The bounds are derived from the global analysis of oscillation data including the effect of NSI in the SNO NC cross section and *assuming only one NSI coupling different from zero at a time*. As explained in section 3.1, these bounds apply to models with $M_{\text{med}} \gtrsim 3 \text{ MeV}$.

respectively. Thus the allowed range for flavour diagonal NSI is formed by two solutions around $\varepsilon_{\alpha\alpha}^{q,A} = 0$ and $\varepsilon_{\alpha\alpha}^{q,A} = -2$. For flavour off-diagonal NSI it is formed by solutions around $\varepsilon_{\alpha\neq\beta}^{q,A} = 0$ and $\varepsilon_{\alpha\neq\beta}^{q,A} = \mp 4 \text{Re}(\rho_{\alpha\neq\beta}^{\text{SNO}}) / (\rho_{\alpha\alpha}^{\text{SNO}} + \rho_{\beta\beta}^{\text{SNO}})$. For $\varepsilon_{e\mu}^{q,A}$ (and similarly for $\varepsilon_{e\tau}^{q,A}$) this last condition corresponds, in fact, to two distinct solutions, both around $|\varepsilon_{e\mu}^{q,A}| \neq 0$ and two possible signs, due to the two different signs of $\rho_{e\mu}^{\text{SNO}}$ for the two CP-conserving values of $\delta_{\text{CP}} \in \{0, \pi\}$. On the contrary, $\rho_{\mu\tau}^{\text{SNO}}$ takes very similar values for $\delta_{\text{CP}} \in \{0, \pi\}$, and consequently for $\varepsilon_{\mu\tau}^{q,A}$ the two non-zero solutions closely overlap around $\varepsilon_{\mu\tau}^{u,A} \sim 1.7$ ($\varepsilon_{\mu\tau}^{d,A} \sim -1.7$).

3.4 Constraints on NSI with quarks and electrons: effective NSI in the Earth

Let us now discuss the most general case in which NSI with quarks and electrons are considered, parametrized by the angles η and ζ introduced in eqs. (2.4) and (2.5). We focus on vector NSI because in this case the interplay between matter and scattering effects, and therefore the dependence on the couplings to charged fermions involved, is expected to play a most relevant role.

In this framework, it is useful to quantify the results of our analysis in terms of the effective NSI parameters which describe the generalized Earth matter potential, which are in fact the relevant quantities for the study of long-baseline and atmospheric oscillation experiments. The results are displayed in figure 6 and on the right column in table 5 where we show the allowed two-dimensional regions and one-dimensional ranges of the effective NSI coefficients for the global analysis of oscillation and CE ν NS data, after marginalizing over all other parameters. Therefore what we quantify in figure 6 and the right column in table 5 is our present knowledge of the matter potential for neutrino propagation in the Earth, for NSI induced by mediators heavier than $M_{\text{med}} \gtrsim 50 \text{ MeV}$ (as discussed in section 3.1) and for *any unknown value* of η and ζ . Technically this is obtained by marginalizing the results of the global χ^2 with respect to η and ζ as well, and the $\Delta\chi^2$ functions plotted in the figure are defined with respect to the absolute minimum for any η and ζ which, lies close to $\eta \sim -45^\circ$ and $\zeta \sim 10^\circ$.

Allowed ranges at 90% CL (99% CL) marginalized		
GLOB-OSC w/o NSI in ES		GLOB-OSC w NSI in ES + CE ν NS
$\epsilon_{ee}^{\oplus} - \epsilon_{\mu\mu}^{\oplus}$	$[-3.1, -2.8] \oplus [-2.1, -1.88] \oplus [-0.15, +0.17]$ ($[-4.8, -1.6] \oplus [-0.40, +2.6]$)	$[-0.19, +0.20] \oplus [+0.95, +1.3]$ ($[-0.23, +0.25] \oplus [+0.81, +1.3]$)
$\epsilon_{\tau\tau}^{\oplus} - \epsilon_{\mu\mu}^{\oplus}$	$[-0.0215, +0.0122]$ ($[-0.075, +0.080]$)	$[-0.43, +0.14] \oplus [+0.91, +1.3]$ ($[-0.29, +0.20] \oplus [+0.83, +1.4]$)
$\epsilon_{e\mu}^{\oplus}$	$[-0.11, -0.021] \oplus [+0.045, +0.135]$ ($[-0.32, +0.40]$)	$[-0.43, +0.14] \oplus [+0.91, +1.3]$ ($[-0.29, +0.20] \oplus [+0.83, +1.4]$)
$\epsilon_{\mu\tau}^{\oplus}$	$[-0.22, +0.088]$ ($[-0.49, +0.45]$)	$[-0.12, +0.011]$ ($[-0.18, +0.08]$)
$\epsilon_{\mu\tau}^{\oplus}$	$[-0.0063, +0.013]$ ($[-0.043, +0.039]$)	$[-0.16, +0.083]$ ($[-0.25, +0.33]$)
$\epsilon_{\mu\tau}^{\oplus}$		$[-0.0047, +0.012]$ ($[-0.020, +0.021]$)

Table 5. 90% and 99% CL bounds (1 d.o.f., 2-sided) on the effective NSI parameters relevant for matter effects in LBL experiments with arbitrary values of η and ζ , obtained after marginalizing over all other NSI and oscillation parameters. The bounds on the left (right) column are applicable to NSI induced by mediators with masses $M_{\text{med}} \ll 500 \text{ keV}$ ($M_{\text{med}} \gtrsim 50 \text{ MeV}$).

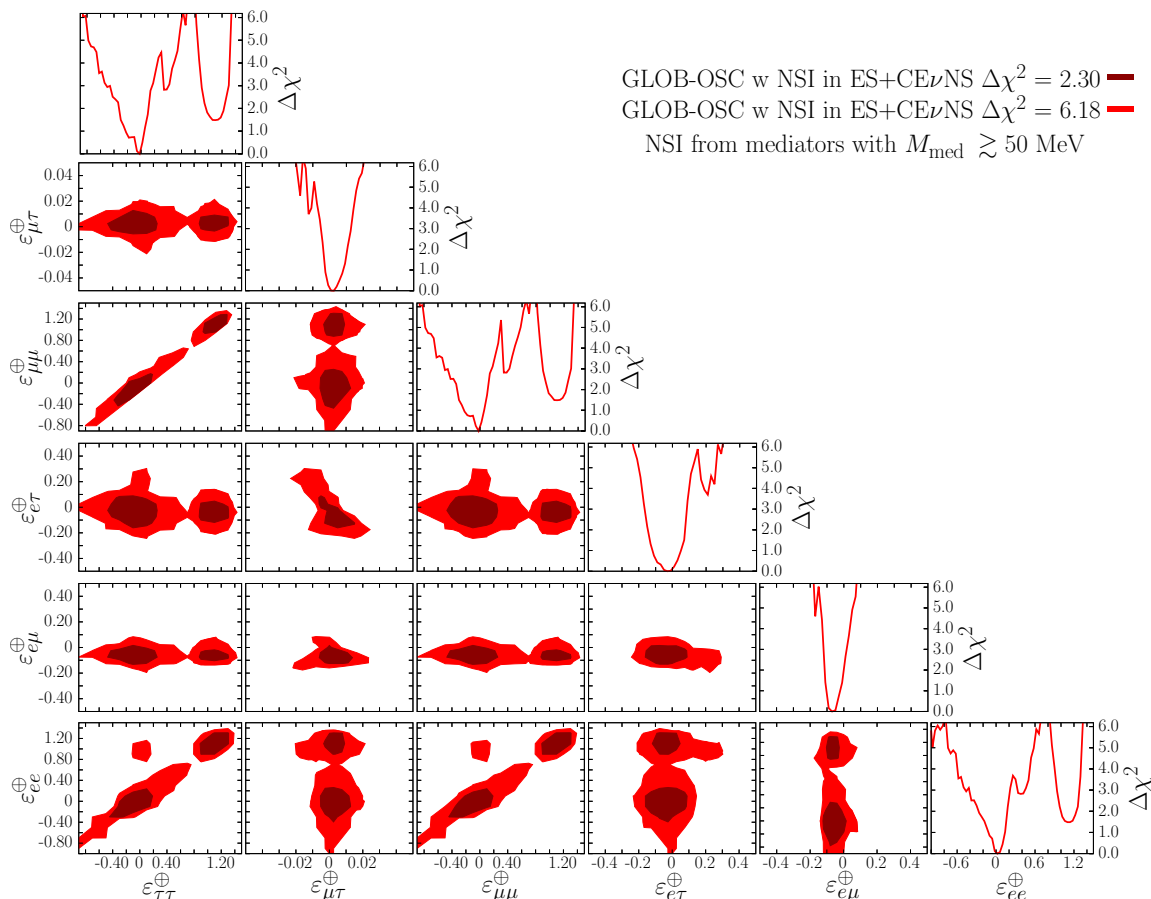


Figure 6. Constraints on the effective generalized NSI in the Earth matter (relevant for matter effects in LBL experiments) with arbitrary values of η and ζ . Each panel shows a two-dimensional projection of the allowed multi-dimensional parameter space after minimization with respect to the undisplayed parameters. The contours correspond to 1σ and 2σ (2 d.o.f.).

From these results we see that the allowed ranges for the diagonal $\varepsilon_{\alpha\alpha}^{\oplus}$ parameters are composed of two disjoint regions. However let us stress that they both correspond to the LMA solution since neither of them falls within the LMA-D region (which requires $\varepsilon_{ee}^{\oplus} - \varepsilon_{\mu\mu}^{\oplus} = -2$). In fact, the LMA-D solution is ruled out beyond the CL shown in figure 6 and, as will be discussed in section 3.5 in more detail, the combination of oscillation data with CE ν NS results for different nuclear targets is required to reach this sensitivity.

Conversely, for mediators with masses $M_{\text{med}} \ll 500$ keV, effects on ES and CE ν NS experiments would be suppressed even if NSI involve couplings to both quarks and electrons, and the only effect of NSI will be the modification of the matter potential in neutrino oscillations. The same holds for NSI with quarks only (i.e., for $\zeta = 0$) induced by mediators with masses $M_{\text{med}} \ll 10$ MeV. Since in the matter potential the effects for protons or electrons are indistinguishable, the allowed ranges of the effective $\varepsilon_{\alpha\beta}^{\oplus}$ are the same in both scenarios, which are given on the left column in table 5 (and included in figure 5). As discussed in section 2.1, in this case the analysis can only constrain the differences between

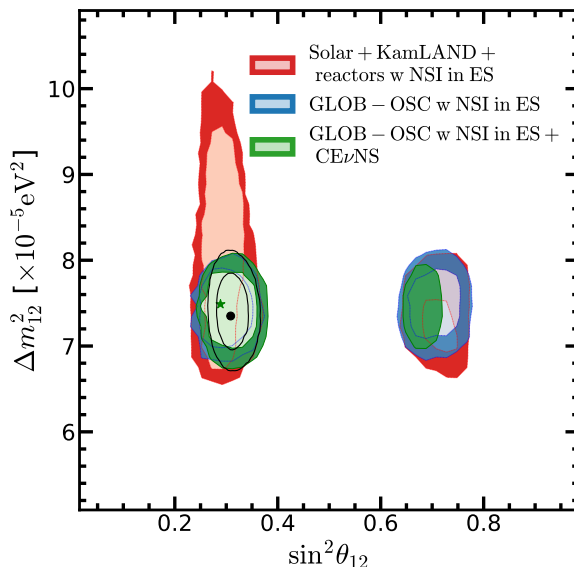


Figure 7. Two-dimensional projections of the allowed regions (at 90% and 3σ CL) onto Δm_{12}^2 and θ_{12} parameters, after marginalizing over all other oscillation parameters and over NSI couplings to quarks and electrons. Red regions correspond to the analysis of KamLAND and Solar data; blue regions include all oscillation data; and green regions include all oscillation and CE ν NS data. In all cases, NSI effects on ES are fully accounted for in the fit. For comparison, the empty contours (solid black lines) show the corresponding regions for the global oscillation analysis without NSI.

flavour-diagonal NSI coefficients. Furthermore, the allowed range of $\varepsilon_{ee}^\oplus - \varepsilon_{\mu\mu}^\oplus$ contains a disjoint interval around -2 (which at 90% CL further splits into two sub-intervals as seen in the table) corresponding to the LMA-D solution, which is well allowed in these scenarios. We will discuss this in more detail in section 3.5.

We finish this section by discussing the impact of NSI in this general framework (where we allow couplings to quarks and electrons simultaneously) on the determination of the oscillation parameters in the solar sector. This is shown in figure 7, where we see that the determination of the oscillation parameters within the LMA region, which is the region favored by the fit, is rather robust even after the inclusion of NSI couplings to both quarks and electrons. Comparing the blue and red regions in the figure we see that the inclusion of data from atmospheric and LBL experiments is important to reach such robustness. This had been previously shown in refs. [28, 29] for NSI with quarks only; here we conclude that the same conclusions hold also in presence of NSI with electrons, as long as their impact on ES is accounted for in the fit. Also, the allowed LMA regions are not very much affected by the addition of the CE ν NS data and it is very close to that of the oscillation analysis without NSI. As also shown in the figure, the LMA-D is only allowed at 97% CL or above (for 2 d.o.f.). The current status of the LMA-D region is discussed in more detail in the next section.

3.5 Present status of the LMA-D solution

In this section, we discuss in more detail the present status of the LMA-D region in light of all available data, for models leading to NSI couplings to quarks and electrons simultaneously. We start by exploring the dependence of the presence of the LMA-D solution on the specific combination of couplings to the charged fermions considered. In order to do so it is convenient to introduce the functions $\chi_{\text{LMA}}^2(\eta, \zeta)$ and $\chi_{\text{LMA-D}}^2(\eta, \zeta)$ which are obtained by marginalizing the χ^2 for a given value of η and ζ over both the oscillation and the matter potential parameters within the regions $\theta_{12} < 45^\circ$ and $\theta_{12} > 45^\circ$, respectively. With this, in the left (central) panels of figure 8 we plot isocontours of the differences $\chi_{\text{LMA}}^2(\eta, \zeta) - \chi_{\text{no-NSI}}^2$ ($\chi_{\text{LMA-D}}^2(\eta, \zeta) - \chi_{\text{no-NSI}}^2$) where $\chi_{\text{no-NSI}}^2$ is the minimum χ^2 for standard 3ν oscillations (i.e., without NSI). In the right panels we plot $\chi_{\text{LMA-D}}^2(\eta, \zeta) - \chi_{\text{LMA}}^2(\eta, \zeta)$ which quantifies the relative quality of the LMA and LMA-D solutions. In each row in this figure we include only a subset of the data as indicated by the labels.

The upper panels of figure 8 show the results when only oscillation data is analyzed accounting for the effects of NSI on the matter potential, but without including the effect of NSI in the ES cross sections in Borexino, SNO, and SK. As outlined in section 3.1, these results would therefore apply to NSI models with very light mediators, $M_{\text{med}} \ll 500$ keV. In this scenario (as shown in section 2.1) only the combination of NSI couplings to electrons, protons and neutrons, parametrized by the effective angle η' in eq. (2.16), is relevant. Therefore the $\Delta\chi^2$ isocontours are curves along $\tan \eta' = \tan \eta / (\cos \zeta + \sin \zeta) = \text{constant}$. From the upper left panel we see that for most of (η, ζ) values, the inclusion of NSI leads only to a mild improvement of the global fit to oscillation data ($\chi_{\text{LMA}}^2(\eta, \zeta) - \chi_{\text{no-NSI}}^2 > -4$). As discussed in ref. [29] (Addendum), with the updated SK4 solar data the determination of Δm_{21}^2 in solar and in KamLAND experiments are fully compatible at $\lesssim 2\sigma$ level. The inclusion of NSI only leads to an overall better fit at a CL above 2σ (but still not statistically significant in any of the different data samples) for (ζ, η) along the darker band. In particular the best fit lies along $\tan \eta' \sim -1/Y_n^\oplus \approx -0.95$ ($\eta' \approx -43.6^\circ$) for which NSI effects in the Earth matter cancel, so there is no constraint from Atmospheric and LBL experiments on the NSI which can lead to that slightly better fit to Solar + KamLAND data within the LMA solution. The central and right panels show the status of the LMA-D solution in this scenario. We find that LMA-D provides a good solution in most of the (η, ζ) plane. The LMA-D is only very disfavoured for (ζ, η) along the band with $2.75 \lesssim \tan \eta' \lesssim -1.75$. For these values the NSI contribution to the matter potential in the Sun cancels in some point inside the neutrino production area and therefore the degeneracy between NSI and the octant of θ_{12} cannot be realized.

The impact of including NSI in the ES cross section in Borexino, SNO, and SK can be seen in the middle row panels in figure 8. Since these panels include the effect of NSI in ES, they apply to NSI models with mediator masses $10 \text{ MeV} \lesssim M_{\text{med}} \lesssim 50 \text{ MeV}$. The main effect is that the ζ values for which the LMA-D solution is allowed become very restricted (in fact the best fit point for all panels are always close to $\zeta = 0$) as long as η does not approach 90° , and consequently the dependence of ζ is heavily suppressed. Thus, once the effect of NSI in the ES cross section is included, the results are not very different from those

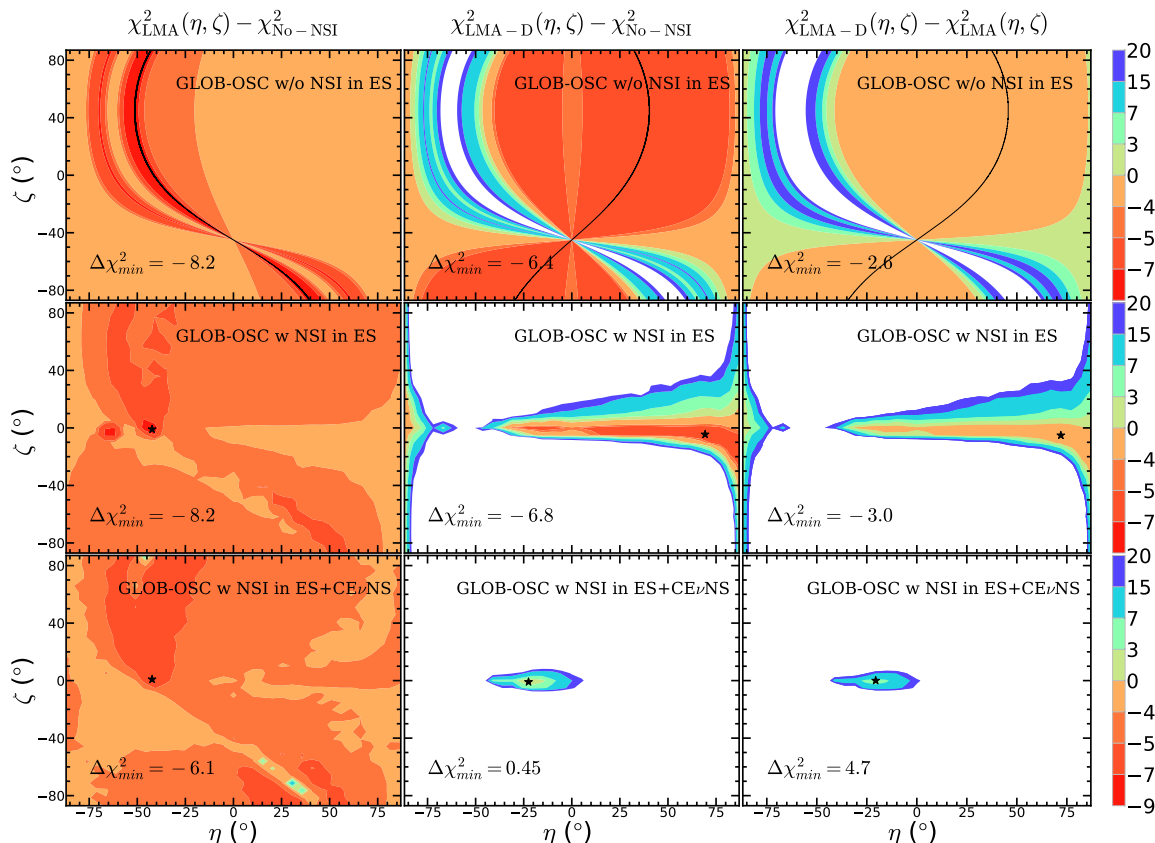


Figure 8. Isocontours of $\chi_{\text{LMA}}^2(\eta, \zeta) - \chi_{\text{no-NSI}}^2$, $\chi_{\text{LMA-D}}^2(\eta, \zeta) - \chi_{\text{no-NSI}}^2$ and $\chi_{\text{LMA-D}}^2(\eta, \zeta) - \chi_{\text{LMA}}^2(\eta, \zeta)$ of the global analysis of oscillation data without including NSI in the ES cross sections at Borexino, SNO, and SK (upper panels), and including the NSI in the ES cross sections at Borexino, SNO, and SK (middle panels). The lower panels shows of the result adding the data from CE ν NS experiments. We show projections in the plane of angles (ζ, η) (after marginalization of all other parameters) which parametrize the relative strength of the NSI couplings to up-quarks, down-quark, and electrons. The levels corresponding to the different colours are given on the color bar on the right. Contours beyond 20 are white. In each panel the best-fit point is marked with a star (middle and bottom rows) or by a solid black line (upper row). Results in the upper row are applicable to NSI induced by mediators with $M_{\text{med}} \ll 500$ keV; in the middle row, for models with $M_{\text{med}} \gtrsim 10$ MeV; and in the lower row, for models with $M_{\text{med}} \gtrsim 50$ MeV, see section 3.1 for details.

obtained for $\zeta = 0$ (no coupling to electrons) in refs. [29, 47]. The middle and right panels in this row also illustrate how, as long as only oscillation data is included, the LMA-D solution is still allowed with a CL comparable and even slightly better than LMA.

The lower panels in figure 8 include the combination of all data available and are therefore applicable to NSI with mediators above $M_{\text{med}} \gtrsim 50$ MeV. When comparing the LMA (LMA-D) to the SM hypothesis (i.e., no NSI) we find that the global minimum of the fit is better (comparable) to that obtained in absence of NSI, as shown in the middle and left panels. However, we also see that the inclusion of the CE ν NS data in the analysis severely constrains the LMA-D solution. Quantitatively we find that LMA-D becomes disfavoured with respect to LMA with $\Delta\chi^2 > 4.7$ for any value of (η, ζ) (right panel) and it

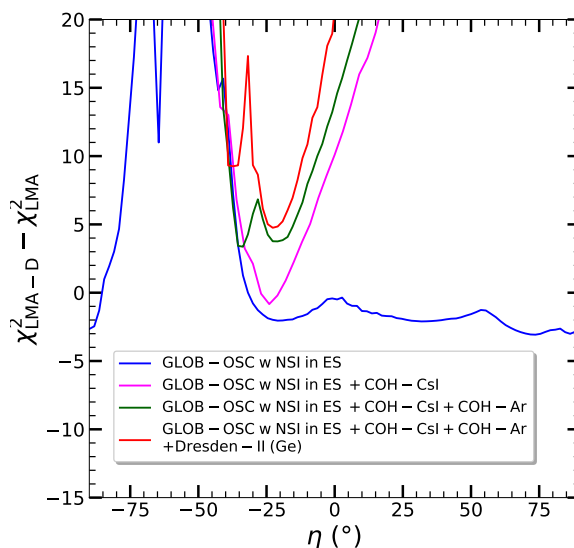


Figure 9. Dependence of $\chi_{\text{LMA-D}}^2(\eta, \zeta) - \chi_{\text{LMA}}^2(\eta, \zeta)$ on η after marginalizing over ζ for different combination of experiments as labeled in the figure.

is only allowed⁷ below $\Delta\chi^2 = 9$ for very specific combinations of couplings to quarks and electrons, $-2.5^\circ \leq \zeta \leq 1.5^\circ$ and $-29^\circ \leq \eta \leq -13^\circ$.

To further illustrate the role of the different experiments in this conclusion we show in figure 9 the projection of $\chi_{\text{LMA-D}}^2(\eta, \zeta) - \chi_{\text{LMA}}^2(\eta, \zeta)$ on η after marginalizing over ζ (which, as discussed above, it is effectively not very different from fixing $\zeta = 0$). The figure illustrates the complementarity of the $\text{CE}\nu\text{NS}$ data with different targets. As discussed in section 2.2.3, the effects of NSI in $\text{CE}\nu\text{NS}$ on a given target, characterized by a value of Y_n , cancel for $\eta'' = \arctan(-1/Y_n)$ (with $\tan \eta'' = \tan \eta / \cos \zeta \simeq \tan \eta$). This corresponds to $\eta \simeq -35.4^\circ$ ($Y_n^{\text{CsI}} \approx 1.407$), -39.3° ($Y_n^{\text{Ar}} \approx 1.222$), and -38.4° ($Y_n^{\text{Ge}} \approx 1.263$) for CsI, Ar, and Ge respectively. Thus, as seen in the figure, the combination of the constraints from $\text{CE}\nu\text{NS}$ with the different targets is important to disfavour the LMA-D solution.

4 Summary

In this work we have presented an updated analysis of neutrino oscillation data and in combination with the results of $\text{CE}\nu\text{NS}$ on a variety of targets with the aim of establishing the allowed size and flavour structure of CP-conserving NC NSI which affect either the evolution of neutrinos in a matter background and/or their detection cross section. We have included in our fit all the latest solar, atmospheric, reactor and accelerator data used for the standard 3ν oscillation analysis in NuFIT-5.2 with the only exception of T2K and NO ν A appearance data whose hints in of CP violation cannot be accommodated within the CP-conserving approximation assumed in this work. When combining with $\text{CE}\nu\text{NS}$

⁷Notice than this is different than what we show in figure 8, where marginalization over η, ζ has been performed.

we include the results from COHERENT data on CSI and Ar detectors, together with the results Dresden-II reactor experiment with a Ge detector.

The study extends previous works by considering either vector or axial NSI with an arbitrary ratio of couplings to up-quarks, down-quarks, and electrons (parametrized by two angles, η and ζ). In the oscillation analysis including vector NSI involving interactions with electrons ($\zeta \neq 0$), which could affect both the propagation and ES detection cross section in Borexino, SNO, and SK, we have consistently accounted for the interplay of flavour transitions in both effects by employing the density matrix formalism (which we had previously proposed). Furthermore we have considered two scenarios: (a) including the NSI only in the matter effects (characteristic of models where NSI are generated by mediators much lighter than $\mathcal{O}(500 \text{ keV})$), and (b) including the NSI both in propagation, CE ν NS, and ES scattering (characteristic of models where NSI are generated by mediators heavier than $\mathcal{O}(50 \text{ MeV})$). Our results show that:

- From the methodological point of view, the validity of the adiabaticity assumption for the neutrino propagation in the Sun in the presence of NSI (and of NP, in general) is not a given. But we conclude that using the adiabatic approximation leads to the correct allowed ranges of NSI coefficients in all cases studied, *as long as one removes from the explored space of NSI couplings those points for which adiabaticity in the Sun is violated.*
- The global oscillation analysis of vector NSI which enter only via the matter potential leads to the bounds on the five combinations $\varepsilon_{ee}^{f,V} - \varepsilon_{\mu\mu}^{f,V}$ and $\varepsilon_{\tau\tau}^{f,V} - \varepsilon_{\mu\mu}^{f,V}$ and $\varepsilon_{\alpha\neq\beta}^{f,V}$ shown in figure 2 and table 1 for interactions with electrons, and in the first column in table 3 for interactions with up and down quark. The 90% bounds range from $\sim 0.5\%$ to $\sim 30\%$ for $\varepsilon_{\tau\tau}^{f,V} - \varepsilon_{\mu\mu}^{f,V}$ and $\varepsilon_{\alpha\neq\beta}^{f,V}$, while $\varepsilon_{ee}^{f,V} - \varepsilon_{\mu\mu}^{f,V}$ presents two (quasi)degenerate allowed ranges around 0 and ~ -2 (~ -1) for NSI with electrons (quarks) which correspond to the well-known LMA and LMA-D solutions.
- The LMA-D solution is realized for generic vector NSI couplings to electrons and quarks as long as only considering propagation effects (see first row in figure 8) unless the couplings come in a ratio that cancels their contribution to the solar matter potential ($2.75 \lesssim \tan \eta / (\cos \zeta + \sin \zeta) \lesssim -1.75$).
- Including the effect of the vector NSI in the ES scattering cross sections in Borexino, SK and SNO, lifts the degeneracy and disfavours the LMA-D solution unless the NSI coupling to the electrons is suppressed compared to the coupling to quarks (see second row in figure 8). But it still provides a good fit to the data for a wide range of ratios of the couplings to up and down quarks, and it is allowed at 3σ for $\eta < -70^\circ$ or $\eta > -40^\circ$ (see figure 9).
- For vector NSI coupling to electrons only, the inclusion of NSI in the ES scattering cross sections eliminates the LMA-D solution and allows for independent determination of the three $\varepsilon_{\alpha\alpha}^{f,V}$. But within the LMA solution, our comparative results show that it is the presence of the NSI in the matter potential which drives the strong constraints.

- For vector NSI coupling mostly to quarks induced by mediators with $M_{\text{med}} \gtrsim 50$ MeV, the combination of the oscillation results with the data from CE ν NS disfavors the LMA-D solution beyond $\sim 2\sigma$ for any value of η and it is only allowed below $\Delta\chi^2 = 9$ for $-29^\circ \leq \eta \leq -13$. (see figures 8 and 9). We find that the combination of CE ν NS with different nuclear targets is important to disfavor the LMA-D solution at that level.
- The determination of the oscillation parameters within the LMA region is rather robust even after the inclusion of NSI couplings to both quarks and electrons as large as allowed by the global oscillation data analysis itself (see figure 7).
- Axial-vector NSI only enter in the analysis via their effects in the interaction of solar neutrinos in Borexino, SNO, and SK when coupling to electrons, or in the NC rate in SNO when coupling to quarks. For interactions with electrons their bounds are notably weaker than those on vector NSI (see figure 4 and table 2). For interactions with quarks they cannot be all independently bounded (see table 4 for one parameter bounds).

Moreover, to quantify the possible implications that generic models leading to NSI may have for future Earth-based facilities, we have projected the results of our analysis in terms of the effective NSI parameters which describe the generalized matter potential in the Earth, relevant for the study of atmospheric and long-baseline neutrino oscillation experiments (see figure 6 and table 5).

To summarize, this work provides the most general study of NSI involving quarks and electrons up to date using neutrino oscillation data and measurements of CE ν NS using neutrinos from spallation and reactor sources. While the scope of this work is restricted to neutrino facilities, dark matter direct detection experiments are rapidly approaching the so-called neutrino floor. If affected by NSI, significant deviations on the expected results may be observable [102–104]. While present experiments are not competitive yet in this regard, the upcoming generation of experiments will soon provide interesting limits on NSI and may offer additional synergies with neutrino oscillation and CE ν NS data [57].

Acknowledgments

We are grateful to E. Fernandez-Martinez for useful discussions on the interference effects between neutrino oscillations and interactions in the presence of NSI. This project is funded by USA-NSF grant PHY-1915093 and by the European Union through the Horizon 2020 research and innovation program (Marie Skłodowska-Curie grant agreement 860881-HIDDeN) and the Horizon Europe programme (Marie Skłodowska-Curie Staff Exchange grant agreement 101086085-ASYMMETRY). It also receives support from grants PID2019-105614GB-C21, PID2019-108892RB-I00, PID2019-110058GB-C21, PID2020-113644GB-I00, “Unit of Excellence Maria de Maeztu 2020–2023” award to the ICC-UB CEX2019-000918-M, and grant IFT “Centro de Excelencia Severo Ochoa” CEX2020-001007-S funded by MCIN/AEI/10.13039/501100011033, as well as from grant 2021-SGR-249 (Generalitat de

Catalunya) and from the “Generalitat Valenciana” grant PROMETEO/2019/087. PC is supported by grant RYC2018-024240-I funded by MCIN/AEI/10.13039/501100011033 and by “ESF Investing in your future”. SU acknowledges support from Generalitat Valenciana through the plan GenT program (CIDEAGENT/2018/019) and from the Spanish MINECO under Grant FPA2017-85985-P. We also acknowledge use of the IFT and IFIC computing facilities (Hydra and SOM clusters).

Open Access. This article is distributed under the terms of the Creative Commons Attribution License ([CC-BY 4.0](https://creativecommons.org/licenses/by/4.0/)), which permits any use, distribution and reproduction in any medium, provided the original author(s) and source are credited.

References

- [1] B. Pontecorvo, *Neutrino Experiments and the Problem of Conservation of Leptonic Charge*, *Zh. Eksp. Teor. Fiz.* **53** (1967) 1717 [[INSPIRE](#)].
- [2] V.N. Gribov and B. Pontecorvo, *Neutrino astronomy and lepton charge*, *Phys. Lett. B* **28** (1969) 493 [[INSPIRE](#)].
- [3] M.C. Gonzalez-Garcia and M. Maltoni, *Phenomenology with Massive Neutrinos*, *Phys. Rept.* **460** (2008) 1 [[arXiv:0704.1800](#)] [[INSPIRE](#)].
- [4] A. Falkowski et al., *EFT at FASER ν* , *JHEP* **10** (2021) 086 [[arXiv:2105.12136](#)] [[INSPIRE](#)].
- [5] V. Bresó-Pla, A. Falkowski, M. González-Alonso and K. Monsálvez-Pozo, *EFT analysis of New Physics at COHERENT*, *JHEP* **05** (2023) 074 [[arXiv:2301.07036](#)] [[INSPIRE](#)].
- [6] A. Falkowski, M. González-Alonso and Z. Tabrizi, *Consistent QFT description of non-standard neutrino interactions*, *JHEP* **11** (2020) 048 [[arXiv:1910.02971](#)] [[INSPIRE](#)].
- [7] A. Falkowski, M. González-Alonso and Z. Tabrizi, *Reactor neutrino oscillations as constraints on Effective Field Theory*, *JHEP* **05** (2019) 173 [[arXiv:1901.04553](#)] [[INSPIRE](#)].
- [8] S. Davidson, C. Pena-Garay, N. Rius and A. Santamaria, *Present and future bounds on nonstandard neutrino interactions*, *JHEP* **03** (2003) 011 [[hep-ph/0302093](#)] [[INSPIRE](#)].
- [9] C. Biggio, M. Blennow and E. Fernandez-Martinez, *General bounds on non-standard neutrino interactions*, *JHEP* **08** (2009) 090 [[arXiv:0907.0097](#)] [[INSPIRE](#)].
- [10] C. Biggio, M. Blennow and E. Fernandez-Martinez, *Loop bounds on non-standard neutrino interactions*, *JHEP* **03** (2009) 139 [[arXiv:0902.0607](#)] [[INSPIRE](#)].
- [11] M.B. Gavela, D. Hernandez, T. Ota and W. Winter, *Large gauge invariant non-standard neutrino interactions*, *Phys. Rev. D* **79** (2009) 013007 [[arXiv:0809.3451](#)] [[INSPIRE](#)].
- [12] S. Antusch, J.P. Baumann and E. Fernandez-Martinez, *Non-Standard Neutrino Interactions with Matter from Physics Beyond the Standard Model*, *Nucl. Phys. B* **810** (2009) 369 [[arXiv:0807.1003](#)] [[INSPIRE](#)].
- [13] P.S. Bhupal Dev et al., *Neutrino Non-Standard Interactions: A Status Report*, *SciPost Phys. Proc.* **2** (2019) 001 [[arXiv:1907.00991](#)] [[INSPIRE](#)].
- [14] K.S. Babu, A. Friedland, P.A.N. Machado and I. Mocioiu, *Flavor Gauge Models Below the Fermi Scale*, *JHEP* **12** (2017) 096 [[arXiv:1705.01822](#)] [[INSPIRE](#)].
- [15] Y. Farzan, *A model for large non-standard interactions of neutrinos leading to the LMA-Dark solution*, *Phys. Lett. B* **748** (2015) 311 [[arXiv:1505.06906](#)] [[INSPIRE](#)].

- [16] Y. Farzan and J. Heeck, *Neutrinophilic nonstandard interactions*, *Phys. Rev. D* **94** (2016) 053010 [[arXiv:1607.07616](#)] [[INSPIRE](#)].
- [17] Y. Farzan and I.M. Shoemaker, *Lepton Flavor Violating Non-Standard Interactions via Light Mediators*, *JHEP* **07** (2016) 033 [[arXiv:1512.09147](#)] [[INSPIRE](#)].
- [18] A. Greljo, P. Stangl, A.E. Thomsen and J. Zupan, *On $(g-2)_\mu$ from gauged $U(1)_X$* , *JHEP* **07** (2022) 098 [[arXiv:2203.13731](#)] [[INSPIRE](#)].
- [19] J. Heeck, M. Lindner, W. Rodejohann and S. Vogl, *Non-Standard Neutrino Interactions and Neutral Gauge Bosons*, *SciPost Phys.* **6** (2019) 038 [[arXiv:1812.04067](#)] [[INSPIRE](#)].
- [20] Y. Farzan, *A model for lepton flavor violating non-standard neutrino interactions*, *Phys. Lett. B* **803** (2020) 135349 [[arXiv:1912.09408](#)] [[INSPIRE](#)].
- [21] N. Bernal and Y. Farzan, *Neutrino nonstandard interactions with arbitrary couplings to u and d quarks*, *Phys. Rev. D* **107** (2023) 035007 [[arXiv:2211.15686](#)] [[INSPIRE](#)].
- [22] K.S. Babu, P.S.B. Dev, S. Jana and A. Thapa, *Non-Standard Interactions in Radiative Neutrino Mass Models*, *JHEP* **03** (2020) 006 [[arXiv:1907.09498](#)] [[INSPIRE](#)].
- [23] M.B. Wise and Y. Zhang, *Effective Theory and Simple Completions for Neutrino Interactions*, *Phys. Rev. D* **90** (2014) 053005 [[arXiv:1404.4663](#)] [[INSPIRE](#)].
- [24] A. Greljo et al., *Muonic force behind flavor anomalies*, *JHEP* **04** (2022) 151 [[arXiv:2107.07518](#)] [[INSPIRE](#)].
- [25] P. Coloma, M.C. Gonzalez-Garcia and M. Maltoni, *Neutrino oscillation constraints on $U(1)'$ models: from non-standard interactions to long-range forces*, *JHEP* **01** (2021) 114 [Erratum *ibid.* **11** (2022) 115] [[arXiv:2009.14220](#)] [[INSPIRE](#)].
- [26] L. Wolfenstein, *Neutrino Oscillations in Matter*, *Phys. Rev. D* **17** (1978) 2369 [[INSPIRE](#)].
- [27] S.P. Mikheyev and A.Y. Smirnov, *Resonance Amplification of Oscillations in Matter and Spectroscopy of Solar Neutrinos*, *Sov. J. Nucl. Phys.* **42** (1985) 913 [[INSPIRE](#)].
- [28] M.C. Gonzalez-Garcia and M. Maltoni, *Determination of matter potential from global analysis of neutrino oscillation data*, *JHEP* **09** (2013) 152 [[arXiv:1307.3092](#)] [[INSPIRE](#)].
- [29] I. Esteban et al., *Updated constraints on non-standard interactions from global analysis of oscillation data*, *JHEP* **08** (2018) 180 [Addendum *ibid.* **12** (2020) 152] [[arXiv:1805.04530](#)] [[INSPIRE](#)].
- [30] J.W.F. Valle, *Resonant Oscillations of Massless Neutrinos in Matter*, *Phys. Lett. B* **199** (1987) 432 [[INSPIRE](#)].
- [31] M.M. Guzzo, A. Masiero and S.T. Petcov, *On the MSW effect with massless neutrinos and no mixing in the vacuum*, *Phys. Lett. B* **260** (1991) 154 [[INSPIRE](#)].
- [32] O.G. Miranda, M.A. Tortola and J.W.F. Valle, *Are solar neutrino oscillations robust?*, *JHEP* **10** (2006) 008 [[hep-ph/0406280](#)] [[INSPIRE](#)].
- [33] M.C. Gonzalez-Garcia, M. Maltoni and J. Salvado, *Testing matter effects in propagation of atmospheric and long-baseline neutrinos*, *JHEP* **05** (2011) 075 [[arXiv:1103.4365](#)] [[INSPIRE](#)].
- [34] P. Bakhti and Y. Farzan, *Shedding light on LMA-Dark solar neutrino solution by medium baseline reactor experiments: JUNO and RENO-50*, *JHEP* **07** (2014) 064 [[arXiv:1403.0744](#)] [[INSPIRE](#)].
- [35] P. Coloma and T. Schwetz, *Generalized mass ordering degeneracy in neutrino oscillation experiments*, *Phys. Rev. D* **94** (2016) 055005 [Erratum *ibid.* **95** (2017) 079903] [[arXiv:1604.05772](#)] [[INSPIRE](#)].

- [36] K. Scholberg, *Prospects for measuring coherent neutrino-nucleus elastic scattering at a stopped-pion neutrino source*, *Phys. Rev. D* **73** (2006) 033005 [[hep-ex/0511042](#)] [[INSPIRE](#)].
- [37] J. Barranco, O.G. Miranda, C.A. Moura and J.W.F. Valle, *Constraining non-standard interactions in $\nu_e e$ or $\bar{\nu}_e e$ scattering*, *Phys. Rev. D* **73** (2006) 113001 [[hep-ph/0512195](#)] [[INSPIRE](#)].
- [38] J. Barranco, O.G. Miranda and T.I. Rashba, *Probing new physics with coherent neutrino scattering off nuclei*, *JHEP* **12** (2005) 021 [[hep-ph/0508299](#)] [[INSPIRE](#)].
- [39] J. Barranco, O.G. Miranda, C.A. Moura and J.W.F. Valle, *Constraining non-standard neutrino-electron interactions*, *Phys. Rev. D* **77** (2008) 093014 [[arXiv:0711.0698](#)] [[INSPIRE](#)].
- [40] A. Bolanos et al., *Probing non-standard neutrino-electron interactions with solar and reactor neutrinos*, *Phys. Rev. D* **79** (2009) 113012 [[arXiv:0812.4417](#)] [[INSPIRE](#)].
- [41] F.J. Escrihuela, O.G. Miranda, M.A. Tortola and J.W.F. Valle, *Constraining nonstandard neutrino-quark interactions with solar, reactor and accelerator data*, *Phys. Rev. D* **80** (2009) 105009 [Erratum *ibid.* **80** (2009) 129908] [[arXiv:0907.2630](#)] [[INSPIRE](#)].
- [42] D.Z. Freedman, *Coherent Neutrino Nucleus Scattering as a Probe of the Weak Neutral Current*, *Phys. Rev. D* **9** (1974) 1389 [[INSPIRE](#)].
- [43] P. Coloma et al., *Curtailling the Dark Side in Non-Standard Neutrino Interactions*, *JHEP* **04** (2017) 116 [[arXiv:1701.04828](#)] [[INSPIRE](#)].
- [44] I.M. Shoemaker, *COHERENT search strategy for beyond standard model neutrino interactions*, *Phys. Rev. D* **95** (2017) 115028 [[arXiv:1703.05774](#)] [[INSPIRE](#)].
- [45] P. Coloma, M.C. Gonzalez-Garcia, M. Maltoni and T. Schwetz, *COHERENT Enlightenment of the Neutrino Dark Side*, *Phys. Rev. D* **96** (2017) 115007 [[arXiv:1708.02899](#)] [[INSPIRE](#)].
- [46] COHERENT collaboration, *Observation of Coherent Elastic Neutrino-Nucleus Scattering*, *Science* **357** (2017) 1123 [[arXiv:1708.01294](#)] [[INSPIRE](#)].
- [47] P. Coloma, I. Esteban, M.C. Gonzalez-Garcia and M. Maltoni, *Improved global fit to Non-Standard neutrino Interactions using COHERENT energy and timing data*, *JHEP* **02** (2020) 023 [Addendum *ibid.* **12** (2020) 071] [[arXiv:1911.09109](#)] [[INSPIRE](#)].
- [48] COHERENT collaboration, *COHERENT Collaboration data release from the first observation of coherent elastic neutrino-nucleus scattering*, [arXiv:1804.09459](#) [[DOI:10.5281/zenodo.1228631](#)] [[INSPIRE](#)].
- [49] COHERENT collaboration, *First Measurement of Coherent Elastic Neutrino-Nucleus Scattering on Argon*, *Phys. Rev. Lett.* **126** (2021) 012002 [[arXiv:2003.10630](#)] [[INSPIRE](#)].
- [50] J. Colaresi et al., *First results from a search for coherent elastic neutrino-nucleus scattering at a reactor site*, *Phys. Rev. D* **104** (2021) 072003 [[arXiv:2108.02880](#)] [[INSPIRE](#)].
- [51] M. Chaves and T. Schwetz, *Resolving the LMA-dark NSI degeneracy with coherent neutrino-nucleus scattering*, *JHEP* **05** (2021) 042 [[arXiv:2102.11981](#)] [[INSPIRE](#)].
- [52] P. Coloma et al., *Bounds on new physics with data of the Dresden-II reactor experiment and COHERENT*, *JHEP* **05** (2022) 037 [[arXiv:2202.10829](#)] [[INSPIRE](#)].
- [53] BOREXINO collaboration, *Constraints on flavor-diagonal non-standard neutrino interactions from Borexino Phase-II*, *JHEP* **02** (2020) 038 [[arXiv:1905.03512](#)] [[INSPIRE](#)].
- [54] P. Coloma et al., *Constraining new physics with Borexino Phase-II spectral data*, *JHEP* **07** (2022) 138 [Erratum *ibid.* **11** (2022) 138] [[arXiv:2204.03011](#)] [[INSPIRE](#)].

- [55] COHERENT collaboration, *COHERENT Collaboration data release from the first detection of coherent elastic neutrino-nucleus scattering on argon*, [arXiv:2006.12659](#) [[DOI:10.5281/zenodo.3903810](#)] [[INSPIRE](#)].
- [56] J. Colaresi et al., *Measurement of Coherent Elastic Neutrino-Nucleus Scattering from Reactor Antineutrinos*, *Phys. Rev. Lett.* **129** (2022) 211802 [[arXiv:2202.09672](#)] [[INSPIRE](#)].
- [57] D.W.P. Amaral, D. Cerdeño, A. Cheek and P. Foldenauer, *A direct detection view of the neutrino NSI landscape*, *JHEP* **07** (2023) 071 [[arXiv:2302.12846](#)] [[INSPIRE](#)].
- [58] Z. Maki, M. Nakagawa and S. Sakata, *Remarks on the unified model of elementary particles*, *Prog. Theor. Phys.* **28** (1962) 870 [[INSPIRE](#)].
- [59] M. Kobayashi and T. Maskawa, *CP Violation in the Renormalizable Theory of Weak Interaction*, *Prog. Theor. Phys.* **49** (1973) 652 [[INSPIRE](#)].
- [60] I. Esteban et al., *Updated fit to three neutrino mixing: exploring the accelerator-reactor complementarity*, *JHEP* **01** (2017) 087 [[arXiv:1611.01514](#)] [[INSPIRE](#)].
- [61] A.M. Dziewonski and D.L. Anderson, *Preliminary reference earth model*, *Phys. Earth Planet. Interiors* **25** (1981) 297 [[INSPIRE](#)].
- [62] A. Friedland, C. Lunardini and M. Maltoni, *Atmospheric neutrinos as probes of neutrino-matter interactions*, *Phys. Rev. D* **70** (2004) 111301 [[hep-ph/0408264](#)] [[INSPIRE](#)].
- [63] J.N. Bahcall, M. Kamionkowski and A. Sirlin, *Solar neutrinos: Radiative corrections in neutrino-electron scattering experiments*, *Phys. Rev. D* **51** (1995) 6146 [[astro-ph/9502003](#)] [[INSPIRE](#)].
- [64] J.N. Bahcall, K. Kubodera and S. Nozawa, *Neutral Current Reactions of Solar and Supernova Neutrinos on Deuterium*, *Phys. Rev. D* **38** (1988) 1030 [[INSPIRE](#)].
- [65] J. Bernabeu, T.E.O. Ericson, E. Hernandez and J. Ros, *Effects of the axial isoscalar neutral current for solar neutrino detection*, *Nucl. Phys. B* **378** (1992) 131 [[INSPIRE](#)].
- [66] J.-W. Chen, K.M. Heeger and R.G.H. Robertson, *Constraining the leading weak axial two-body current by SNO and super-K*, *Phys. Rev. C* **67** (2003) 025801 [[nucl-th/0210073](#)] [[INSPIRE](#)].
- [67] I. Esteban, M.C. Gonzalez-Garcia, M. Maltoni, T. Schwetz and A. Zhou, *NuFIT 5.2 (2022)*, <http://www.nu-fit.org>.
- [68] B.T. Cleveland et al., *Measurement of the solar electron neutrino flux with the Homestake chlorine detector*, *Astrophys. J.* **496** (1998) 505 [[INSPIRE](#)].
- [69] F. Kaether et al., *Reanalysis of the GALLEX solar neutrino flux and source experiments*, *Phys. Lett. B* **685** (2010) 47 [[arXiv:1001.2731](#)] [[INSPIRE](#)].
- [70] SAGE collaboration, *Measurement of the solar neutrino capture rate with gallium metal. III: Results for the 2002–2007 data-taking period*, *Phys. Rev. C* **80** (2009) 015807 [[arXiv:0901.2200](#)] [[INSPIRE](#)].
- [71] SUPER-KAMIOKANDE collaboration, *Solar neutrino measurements in super-Kamiokande-I*, *Phys. Rev. D* **73** (2006) 112001 [[hep-ex/0508053](#)] [[INSPIRE](#)].
- [72] SUPER-KAMIOKANDE collaboration, *Solar neutrino measurements in Super-Kamiokande-II*, *Phys. Rev. D* **78** (2008) 032002 [[arXiv:0803.4312](#)] [[INSPIRE](#)].
- [73] SUPER-KAMIOKANDE collaboration, *Solar neutrino results in Super-Kamiokande-III*, *Phys. Rev. D* **83** (2011) 052010 [[arXiv:1010.0118](#)] [[INSPIRE](#)].

- [74] Y. Nakajima, *Recent results and future prospects from Super-Kamiokande*, talk given at the *XXIX International Conference on Neutrino Physics and Astrophysics*, Chicago, IL, U.S.A., June 22–July 2, 2020 (online conference).
- [75] SNO collaboration, *Determination of the ν_e and total 8B solar neutrino fluxes with the Sudbury neutrino observatory phase I data set*, *Phys. Rev. C* **75** (2007) 045502 [[nucl-ex/0610020](#)] [[INSPIRE](#)].
- [76] SNO collaboration, *Electron energy spectra, fluxes, and day-night asymmetries of 8B solar neutrinos from measurements with NaCl dissolved in the heavy-water detector at the Sudbury Neutrino Observatory*, *Phys. Rev. C* **72** (2005) 055502 [[nucl-ex/0502021](#)] [[INSPIRE](#)].
- [77] SNO collaboration, *An Independent Measurement of the Total Active 8B Solar Neutrino Flux Using an Array of 3He Proportional Counters at the Sudbury Neutrino Observatory*, *Phys. Rev. Lett.* **101** (2008) 111301 [[arXiv:0806.0989](#)] [[INSPIRE](#)].
- [78] SNO collaboration, *Combined Analysis of all Three Phases of Solar Neutrino Data from the Sudbury Neutrino Observatory*, *Phys. Rev. C* **88** (2013) 025501 [[arXiv:1109.0763](#)] [[INSPIRE](#)].
- [79] G. Bellini et al., *Precision measurement of the 7Be solar neutrino interaction rate in Borexino*, *Phys. Rev. Lett.* **107** (2011) 141302 [[arXiv:1104.1816](#)] [[INSPIRE](#)].
- [80] BOREXINO collaboration, *Measurement of the solar $8B$ neutrino rate with a liquid scintillator target and 3 MeV energy threshold in the Borexino detector*, *Phys. Rev. D* **82** (2010) 033006 [[arXiv:0808.2868](#)] [[INSPIRE](#)].
- [81] BOREXINO collaboration, *First Simultaneous Precision Spectroscopy of pp , 7Be , and pep Solar Neutrinos with Borexino Phase-II*, *Phys. Rev. D* **100** (2019) 082004 [[arXiv:1707.09279](#)] [[INSPIRE](#)].
- [82] KAMLAND collaboration, *Reactor On-Off Antineutrino Measurement with KamLAND*, *Phys. Rev. D* **88** (2013) 033001 [[arXiv:1303.4667](#)] [[INSPIRE](#)].
- [83] DAYA BAY collaboration, *Improved Measurement of the Reactor Antineutrino Flux and Spectrum at Daya Bay*, *Chin. Phys. C* **41** (2017) 013002 [[arXiv:1607.05378](#)] [[INSPIRE](#)].
- [84] T. Bezerra, *New Results from the Double Chooz Experiment*, talk given at the *XXIX International Conference on Neutrino Physics and Astrophysics*, Chicago, IL, U.S.A., June 22–July 2, 2020 (online conference).
- [85] DAYA BAY collaboration, *Precision Measurement of Reactor Antineutrino Oscillation at Kilometer-Scale Baselines by Daya Bay*, *Phys. Rev. Lett.* **130** (2023) 161802 [[arXiv:2211.14988](#)] [[INSPIRE](#)].
- [86] J. Yoo, *RENO*, talk given at the *XXIX International Conference on Neutrino Physics and Astrophysics*, Chicago, IL, U.S.A., June 22–July 2, 2020 (online conference).
- [87] SUPER-KAMIOKANDE collaboration, *Atmospheric Results from Super-Kamiokande*, *AIP Conf. Proc.* **1666** (2015) 100001 [[arXiv:1412.5234](#)] [[INSPIRE](#)].
- [88] ICECUBE collaboration, *Determining neutrino oscillation parameters from atmospheric muon neutrino disappearance with three years of IceCube DeepCore data*, *Phys. Rev. D* **91** (2015) 072004 [[arXiv:1410.7227](#)] [[INSPIRE](#)].
- [89] ICECUBE collaboration, *IceCube Oscillations: 3 years muon neutrino disappearance data*, http://icecube.wisc.edu/science/data/nu_osc.

- [90] ICECUBE collaboration, *Searches for Sterile Neutrinos with the IceCube Detector*, *Phys. Rev. Lett.* **117** (2016) 071801 [[arXiv:1605.01990](#)] [[INSPIRE](#)].
- [91] MINOS collaboration, *Measurement of Neutrino and Antineutrino Oscillations Using Beam and Atmospheric Data in MINOS*, *Phys. Rev. Lett.* **110** (2013) 251801 [[arXiv:1304.6335](#)] [[INSPIRE](#)].
- [92] P. Dunne, *Latest Neutrino Oscillation Results from T2K*, talk given at the *XXIX International Conference on Neutrino Physics and Astrophysics*, Chicago, IL, U.S.A., June 22–July 2, 2020 (online conference).
- [93] A. Himmel, *New Oscillation Results from the NOvA Experiment*, talk given at the *XXIX International Conference on Neutrino Physics and Astrophysics*, Chicago, IL, U.S.A., June 22–July 2, 2020 (online conference).
- [94] J.I. Collar, A.R.L. Kavner and C.M. Lewis, *Response of CsI/NaI to Nuclear Recoils: Impact on Coherent Elastic Neutrino-Nucleus Scattering (CEνNS)*, *Phys. Rev. D* **100** (2019) 033003 [[arXiv:1907.04828](#)] [[INSPIRE](#)].
- [95] P. Klos, J. Menéndez, D. Gazit and A. Schwenk, *Large-scale nuclear structure calculations for spin-dependent WIMP scattering with chiral effective field theory currents*, *Phys. Rev. D* **88** (2013) 083516 [*Erratum ibid.* **89** (2014) 029901] [[arXiv:1304.7684](#)] [[INSPIRE](#)].
- [96] R.H. Helm, *Inelastic and Elastic Scattering of 187-MeV Electrons from Selected Even-Even Nuclei*, *Phys. Rev.* **104** (1956) 1466 [[INSPIRE](#)].
- [97] J.I. Collar, A.R.L. Kavner and C.M. Lewis, *Germanium response to sub-keV nuclear recoils: a multipronged experimental characterization*, *Phys. Rev. D* **103** (2021) 122003 [[arXiv:2102.10089](#)] [[INSPIRE](#)].
- [98] M.C. Gonzalez-Garcia, P.C. de Holanda, E. Masso and R. Zukanovich Funchal, *Probing long-range leptonic forces with solar and reactor neutrinos*, *JCAP* **01** (2007) 005 [[hep-ph/0609094](#)] [[INSPIRE](#)].
- [99] F. Feroz, M.P. Hobson, E. Cameron and A.N. Pettitt, *Importance Nested Sampling and the MultiNest Algorithm*, *Open J. Astrophys.* **2** (2019) 10 [[arXiv:1306.2144](#)] [[INSPIRE](#)].
- [100] F. Feroz, M.P. Hobson and M. Bridges, *MultiNest: an efficient and robust Bayesian inference tool for cosmology and particle physics*, *Mon. Not. Roy. Astron. Soc.* **398** (2009) 1601 [[arXiv:0809.3437](#)] [[INSPIRE](#)].
- [101] GAMBIT collaboration, *Comparison of statistical sampling methods with ScannerBit, the GAMBIT scanning module*, *Eur. Phys. J. C* **77** (2017) 761 [[arXiv:1705.07959](#)] [[INSPIRE](#)].
- [102] D.G. Cerdeño et al., *Physics from solar neutrinos in dark matter direct detection experiments*, *JHEP* **05** (2016) 118 [*Erratum ibid.* **09** (2016) 048] [[arXiv:1604.01025](#)] [[INSPIRE](#)].
- [103] C. Boehm et al., *How high is the neutrino floor?*, *JCAP* **01** (2019) 043 [[arXiv:1809.06385](#)] [[INSPIRE](#)].
- [104] M.C. Gonzalez-Garcia, M. Maltoni, Y.F. Perez-Gonzalez and R. Zukanovich Funchal, *Neutrino Discovery Limit of Dark Matter Direct Detection Experiments in the Presence of Non-Standard Interactions*, *JHEP* **07** (2018) 019 [[arXiv:1803.03650](#)] [[INSPIRE](#)].